NRLMSISE-00 EMPIRICAL MODEL OF THE ATMOSPHERE: STATISTICAL COMPARISONS AND SCIENTIFIC ISSUES

J. M. Picone, A. E. Hedin[1], and D. P. Drob

E. O. Hulburt Center for Space Research
Naval Research Laboratory
Washington, DC 20375

A. C. Aikin

Laboratory for Atmospheres
NASA Goddard Space Flight Center
Greenbelt, Maryland 20771

Submitted to:

Journal of Geophysical Research

December 2001

[1] Universities Space Research Association, Washington, DC 20024-4703

ABSTRACT

The new NRLMSISE-00 model and the associated NRLMSIS database now include the following data: (1) total mass density from satellite accelerometers and from orbit determination, including the Jacchia and Barlier data; (2) temperature from incoherent scatter radar, and; (3) molecular oxygen number density, $[O_2]$, from solar ultraviolet occultation aboard the Solar Maximum Mission (SMM). A new component, "anomalous oxygen," allows for appreciable O^+ and hot atomic oxygen contributions to the total mass density at high altitudes and applies primarily to drag estimation above 500 km. Extensive tables compare our entire database to the NRLMSISE-00, MSISE-90, and Jacchia-70 models for different altitude bands and levels of geomagnetic activity. We also investigate scientific issues related to the new data sets in the NRLMSIS database. Especially noteworthy is the solar activity dependence of the Jacchia data, with which we investigate a large O^+ contribution to the total mass density under the combination of summer, low solar activity, high latitudes, and high altitudes. Under these conditions, except at very low solar activity, the Jacchia data and the Jacchia-70 model indeed show a significantly higher total mass density than does MSISE-90. However, under the corresponding winter conditions, the MSIS-class models represent a noticeable improvement relative to Jacchia-70 over a wide range of $F_{10.7}$. Considering the two regimes together, NRLMSISE-00 achieves an improvement over both MSISE-90 and Jacchia-70 by incorporating advantages of each.

1. Introduction

The NRLMSISE-00 empirical model of thermospheric composition and temperature is now available for access and use by the scientific and operational communities (Appendex, subsection A.4). This paper compares the new model to the standard scientific (MSISE-90 [Hedin, 1991]) and operational (Jacchia-70 [Jacchia, 1970]) empirical models presently in use, through statistical comparison with the previous MSIS database and with the newly added data sets that make NRLMSISE-00 unique. We then address scientific issues related to the newly added data.

This milestone fulfills our initial goal of preserving and continuing the line of MSIS-class models. Empirical models of the thermosphere and upper mesosphere are an indispensable tool used by the operational and upper atmospheric research communities for data analysis, initialization of detailed physics-based models, and mission and instrument design. For over a decade, the models of choice among scientists have been the Mass Spectrometer - Incoherent Scatter Radar (MSIS-class) models of upper atmospheric composition and temperature: MSIS-86 [Hedin, 1987], which ranges upward from 90 km, and MSISE-90, which extends from the ground to the exobase. Some research communities continue to use the CIRA-86 climatology, which consists of two overlapping specifications: tables generated from MSIS-86 for the thermosphere (altitude $z > 100$ km; http://nssdc.gsfc.nasa.gov/space/model/atmos/cospar2.html)) and tables based on averages of global data compilations for the mesosphere and below ($z < 120$ km; http://nssdc.gsfc.nasa.gov/space/model/atmos/cospar1.html). Operational communities use the Jacchia-class models or in some cases, the extremely limited US Standard Atmosphere (http://nssdc.gsfc.nasa.gov/space/model/atmos/us_standard.html). The database underlying operational Jacchia models (1970 and earlier) consists of total mass density derived from orbital decay of objects which flew during the 1961-70. Past MSIS-class models derived from over two-decades of data on composition, temperature, and total mass density, rather than from orbital dynamics.

For estimating total mass density, the NRLMSISE-00 model and its underlying database are at least comparable to the Jacchia-class models, given the inclusion of numerous orbital drag (F. Barlier, private communication to A. Hedin) and accelerometer data sets (F. Marcos, private communication). A noteworthy addition to the database is the actual orbital decay data on which

the Jacchia models are primarily based. The model also incorporates recent data on temperature and molecular oxygen number density, $[O_2]$. The new data sets are extensive in size, spatial range and the time period covered and represent significant departures from the MSIS database used to produce previous generations of the model.

This upgrade is important because the MSIS and Jacchia models do not depend on calendar year and cannot directly track any gradual changes in the atmosphere due to anthropogenic or solar influences. The only way in which empirical models can maintain currency with the recent state of the atmosphere is by continually adding recent data to the database and then modifying the parameter set. In addition, instrumentation and data processing methods have improved and have become more diverse, potentially allowing the addition of higher order terms and reducing the uncertainty of the model coefficients. To accommodate new data, the formulation of the model and the methodology for generating it have become more robust (Appendix).

One change is particularly worthy of mention. The inclusion of drag data in a neutral atmospheric model has required us to account explicitly for high altitude O^+ and hot atomic oxygen components, which might contribute appreciably to drag under some conditions (Section 4.1). As a result, the NRLMSIS formulation now explicitly includes a component, called "anomalous oxygen," to account the contribution of these species to satellite drag at high altitudes and permits the user to compute both the "thermospheric mass density" (or "total neutral mass density") provided by past generations of MSIS and an "effective" mass density, which denotes the sum of the thermospheric mass density and the anomalous oxygen contribution at altitudes near the exobase.

To introduce the new model, Section 2 describes the newly added data sets and their relationship to the previous database. Section 3 presents statistical comparisons of NRLMSISE-00, MSISE-90, and Jacchia-70 with the NRLMSIS database. The statistical tables significantly augment a previous report on drag and accelerometer data [Hedin, 1988]. Section 4 discusses important scientific issues related to the new data and model, and Section 5 discusses our conclusions regarding NRLMSISE-00 and the direction of future development. The Appendix summarizes the formulation, generation, and access of the new model and addresses the use of orbital drag and accelerometer data to generate NRLMSISE-00.

2. The NRLMSIS database and model

2.1. Relationship to past models

NRLMSISE-00 retains the calling sequence and arguments of MSISE-90 and earlier MSIS models. In the remainder of the paper, we will often exclude the designation "E-00" for the sake of brevity. One can usefully interpret the NRLMSIS model as a flexible, semi-empirical view of its extensive underlying database. That is, the model takes statistical variability into account while interpolating among, or extrapolating, the underlying data sets to estimate composition and temperature for times, geophysical conditions, and locations not covered specifically by the database. As with earlier versions of the MSIS-class models, the NRLMSIS database includes ground-, rocket-, and satellite-based measurements. The data underlying MSISE-90 cover the period 1965-83 and derive from incoherent scatter radar (ISR), mass spectrometer, solar ultraviolet (UV) occultation, pressure gauge, falling sphere, and grenade detonations. Until now, the database has not included either drag measurements, on which the Jacchia models were based, or satellite-borne accelerometer data. The new NRLMSIS upgrade includes those data sets.

Both the MSIS and Jacchia models are sensitive to the level of geomagnetic activity and provide an estimate of the average upper atmospheric state under geomagnetic storm conditions. However, at high latitudes and high geomagnetic activity, the databases are sparse, and as statistical averages the models do not capture the local structure and shorter time scales associated with any particular storm. The NRLMSISE-00 model remains a statistical average, but the database now contains more data covering extremes of location and forcing.

2.2. Expanded database

The most important upgrade has been the addition of recent data sets and new categories of data to augment the NRLMSIS database and model:

(a) Satellite drag [Jacchia, 1970; Barlier, 1978; Hedin, 1988]: orbit determination (1961-1971);

(b) Accelerometer (Hedin, 1988; F. Marcos, private communication): Atmospheric Explorer (AE-C, D, E) MESA [Champion and Marcos, 1973], Air Force SETA [Rhoden et al., 2000], CACTUS [Boudon et al., 1979], San Marco-5 [Arduini et al., 1997]];

(c) Incoherent scatter radar (ISR) - exospheric temperature (T_{ex}): Millstone Hill (1981-97; [Buonsanto and Pohlman, 1998]), Arecibo (1985-95; [Melendez-Alvira et al., 1998]

(d) ISR - Lower thermospheric temperature (T_{low}): Millstone Hill (1988-97; Goncharenko and Salah [1998].

(e) Solar Maximum Mission (SMM) O_2 density data derived from occultation of solar UV emissions [Aikin et al., 1993].

Ingesting the drag and accelerometer data on total mass density (ρ) promises to remove a postulated deficiency of MSIS for orbital tracking applications. With the inclusion of the Jacchia data, the more extensive and well-documented NRLMSIS database should equal or improve the statistical predictions of ρ and of drag over those of the Jacchia models. We expect to test this hypothesis by applying the model to operational precision orbit determination and prediction [Knowles et al., 2001]. An important point is that the new data on total mass density also influence the model coefficients for both temperature and composition. These differences should become apparent as NRLMSIS is compared to additional data sets.

The incoherent scatter radar data directly influence the model temperature, which is the core of the MSIS formulation. Further, the new data cover an appreciable fraction of a solar cycle or more and are vital for both testing the existing models and producing new versions. The methods of processing ISR data have also undergone significant improvements over the last decade, increasing the quality of the inferred ionospheric properties [Gonzales and Sulzer, 1996]. This factor imparts high value to our new data sets.

The Millstone Hill data on lower thermospheric temperature (T_{low}) cover 100 km $\leq z \leq$130 km [Goncharenko and Salah, 1998]. In this regime, the neutral temperature is approximately equal to the ion temperature, so that extraction of the information is straightforward. These high quality data permit us to check and reinforce key MSIS temperature model parameters and ~~will be~~ these data are important in defining the model at the mesopause.

The SMM mission provided data on the molecular oxygen number density [O_2] over the altitude range 140-200 km and over a wide range of solar activity. Prior to SMM, direct measurements of [O_2] above 150 km were not available at high solar activity. The SMM occultation measurements suggest that dissociation may increase sufficiently to keep this density

nearly constant at 200 km as solar activity increases [Kayser, 1980; Aikin et al, 1993]. These data are now part of the NRLMSIS database and will be important in determining dependence on the solar extreme ultraviolet (EUV) flux and on magnetic activity. As a result, the data should be particularly useful in future analysis of better EUV proxies (e.g., Lean et al. [2001]). On the other hand, the longstanding conflict between mass spectrometer and solar UV occultation measurements of thermospheric $[O_2]$ has had a profound effect on NRLMSIS, because the occultation data do not follow diffusive equilibrium, contradicting mass spectrometer data [Aikin et al., 1993]. At the same time, the latter could be biased toward high values by recombination of atomic oxygen within the instrument. As an example, the two sources disagree on average by a factor of two or more at 200 km. The SMM data set has therefore required alterations in the formulation of NRLMSIS (see Appendix) and has significantly influenced the dependence of $[O_2]$ estimates on $F_{10.7}$ (Section 4.2).

3. Statistical comparisons of models to data

A key component of this paper is the presentation of coarse statistical measures (bias, β, and standard deviation, σ) to gauge the agreement of the commonly used empirical upper atmospheric models (MSISE-90 and, Jacchia-70) and the new model, NRLMSISE-00, with the NRLMSIS database. Generally, the bias is the weighted mean of the residuals $\{d_i - m_i\}$ between the data set $\{d_i\}$ and the corresponding model estimates $\{m_i\}$, thereby measuring their systematic differences. The weighting factor for a given data point is the squared reciprocal of the attributed error, and angle brackets "$\langle\ \rangle$" denote the weighted mean. Positive bias (β) indicates that a model underestimates the measured density values on average while negative bias signifies overestimation. The standard deviation is $(\langle(d_i - m_i)^2\rangle - \beta^2)^{1/2}$ and measures a model's coverage of the time scales and phases implicit in the data. However, σ also reflects the noise implicit in the data sets, so that the standard deviation can be somewhat ambiguous. When the three models are compared with identical data sets, the relative values of σ should give an indication of the agreement of the various models with measured time scales and the associated phases.

The NRLMSIS database consists of two components: the complete data sets acquired from the various sources and the subset of data "selected" to generate the model. Hedin et al. [1977] described the selection process, which was designed to ensure the widest coverage of the hyperspace of subroutine arguments while satisfying constraints imposed by computing and

storage limitations. Hedin's method also avoids dominance of the model coefficients by only a few large data sets, although this can also be accomplished by proper weighting of data-model residuals in computing χ^2. In order to insure against domination of NRLMSISE-00 by the new data sets and to maintain consistency with past MSIS versions, we have performed a similar selection from the new data.

The tables of (β, σ) values include both the model generation database and the complete, newly added data sets. For temperature T, the tables show $\beta \equiv \langle T_i(\text{data}) - T_i(\text{model}) \rangle$ and $\sigma \equiv (\langle [T_i(\text{data}) - T_i(\text{model})]^2 \rangle - \beta^2)^{1/2}$. For species number density and total mass density, we have computed the bias as $\beta = \exp(\log_e(\rho_i(\text{data})/\rho_i(\text{model})) - 1$ to provide an average fractional density bias and have computed the standard deviation as $\sigma = (\langle \log_e^2\{\rho_i(\text{data})/\rho_i(\text{model})\}\rangle - \beta^2)^{1/2}$. The number of tables is sufficiently large that they have been placed in the AGU Electronic Dataset Archive for access by interested readers. In our discussion below, we denote these tables by A1(a)-(c) to A9(a)-(c), where "A" signifies "archive" and (a)-(c) denote, respectively, quiet ($A_p \leq 10$) and active ($A_p \geq 50$) geomagnetic conditions and the union of all geomagnetic conditions ("all" data). The tables abbreviate the names of the models to N00 (NRLMSISE-00), M90 (MSISE-90), and J70 (Jacchia-70). The tables cover total mass density (ρ), temperature, and individual species (excluding anomalous oxygen). For the tables relating to quiet conditions and to all data, the calculations used only data points deviating from the new model by 15 × the associated error, or less. For active conditions, the database was sufficiently sparse that all high activity points were used to construct the tables. Finally, for "all" and $A_p \geq 50$, we used the 3 hr a_p inputs to the NRLMSISE-00 ("N00") and MSISE-00 ("M90") models, while for quiet conditions, we used the daily A_p input.

The bias and standard deviation are coarse measures, and are useful primarily for simple error analysis. Statistical differences among models often appear to be moderate and are not consistent across all data sources, potentially masking trends and systematic differences. Relative to our database, the most obvious differences among the models involve the standard deviation of the model-data residuals. While σ is comparable among the models regarding temperature and total mass density, NRLMSISE-00 shows better performance for composition, especially as altitude increases. The latter effect also occurs for exospheric temperature but is not pronounced. For Jacchia-70, the best temperature results relative to the MSIS-class models occurred for the

combination of lower altitudes and satellite-based observations. At high geomagnetic activity, comparisons with the data showed similar or degraded performance of all models relative to the low geomagnetic activity cases.

Consideration of key drivers or variations makes the differences among models more apparent (e.g., see the next section on variations with the solar EUV flux, as represented by $F_{10.7}$). In addition, comparisons of the models for selected data sets can sometimes be illuminating, if the user has knowledge of those particular data sets, if the data sets derive from the same or similar sources, or if particular altitude or geomagnetic activity ranges are emphasized. As an example and as an introduction to Section 4.1 on anomalous oxygen contributions to total mass density, Table 1 below compares the Jacchia data set to the three models. As indicated above, the table shows that the biases and standard deviations of the three models are comparable in magnitude; this is especially true for ρ, across all accelerometer and drag data sets. However, two additional, secondary features appear. First, the Jacchia model shows a consistent negative bias, on average overestimating the Jacchia data. Section 4.1 shows that this is likely attributable to a nonoptimal match with $F_{10.7}$ variability of the data. Second, at high geomagnetic activity, the standard deviations of the M90 and J70 models are consistently higher than that of NRLMSIS. This suggests that the new model handles spatial and seasonal variability somewhat better than the other models at elevated geomagnetic activity. In neither case, however, does β or σ allow us to make a strong inference.

Table 1

STATISTICAL COMPARISON OF EMPIRICAL MODELS TO JACCHIA DATA

A_p	Altitude	Points	N00		M90		J70	
			β	σ	β	σ	β	σ
≤ 10	200 - 400	6236	-0.06	0.17	-0.06	0.17	-0.04	0.17
	400 - 800	10041	-0.07	0.23	-0.08	0.26	-0.07	0.25
	800 - 1200	5586	0.01	0.23	0.03	0.27	-0.05	0.23
	> 1200	15	0.20	0.09	0.27	0.10	-0.18	0.05
All	200 - 400	10456	-0.07	0.17	-0.06	0.17	-0.07	0.19
	400 - 800	16021	-0.08	0.25	-0.07	0.27	-0.09	0.28
	800 - 1200	9373	0.01	0.24	0.04	0.27	-0.07	0.25

	> 1200	24	0.22	0.12	0.30	0.11	-0.20	0.13
≥ 50	200 - 400	304	-0.05	0.23	-0.07	0.23	-0.12	0.25
	400 - 800	441	-0.01	0.36	0.01	0.39	-0.17	0.42
	800 - 1200	282	0.07	0.35	0.05	0.39	-0.14	0.39

4. Scientific and technical issues

4.1. Anomalous oxygen and solar activity

4.1.1. Background

As shown by Hedin [1989], both the Jacchia model and data from the neutral mass spectrometer aboard Dynamics Explorer-2 (DE-2) indicated that an appreciable hot atomic oxygen population could be present at high latitudes and altitudes (> 600 km) during the summer. The DE-2 measurements showed an elevated oxygen component under moderate to high solar activity, consistent with suggestions by Yee et al [1980]. that a hot oxygen geocorona might exist with temperature of ~ 4000 K. For low solar activity, at high altitudes and summer high latitudes, the Jacchia-70 model showed significantly higher total mass density (and helium concentration) than did MSIS-86. Hedin hypothesized that a hot oxygen geocorona could cause these discrepancies.

Recent analyses of ISR data by Oliver [1997] and Oliver and Schoendorf [1999] have argued for a small, but non-negligible, hot oxygen component (emphasizing altitudes around 400 km), especially at night and at the solstices during solar minimum. Schoendorf et al.[2000] have developed model profiles of hot oxygen for use in analyzing incoherent scatter radar data, e.g., to derive T_{ex} (Section 4.3). While the ISR sites are somewhat lower in latitude than our region of interest (see below), a broadening of the investigations by Oliver et al. should significantly augment the present understanding of the hot oxygen component and could guide our future upgrades of NRLMSIS.

The emphasis on hot atomic oxygen changed significantly when Keating et al. [1998] analyzed neutral and ion mass spectrometer measurements aboard the Midcourse Space Experiment (MSX), which flew in a sun-synchronous (near-polar) circular orbit at approximately 900 km during the most recent solar minimum. Based on comparisons of the Jacchia-70 and

MSIS-86 models, similar to those of Hedin, Keating et al. showed that the measured O^+ concentration could account for the discrepancy in the respective model estimates of [He] and total mass density.

In response to these developments, the NRLMSIS model now includes an "anomalous oxygen" (AO) component, which represents any appreciable, persistent O^+ and hot O populations at higher altitudes (> 500 km). The functional form of the anomalous oxygen model profile is similar to that of an isothermal Chapman layer, with an adjustable magnitude and scale height (or temperature; Appendix A.1). The data used to evaluate these parameters were simply the Jacchia and Barlier (JB) data above 600 km. At the same time, we excluded the summer JB data above 600 km from the data sets used to determine the He and "cold" O components of the model. While the winter data above 600 km are common to He, cold O, and anomalous O, our tests have shown small differences between NRLMSISE-00 and MSISE-90 for these data, indicating less influence of the additional oxygen component on the new model during winter at high altitudes. Surprisingly, the Jacchia –70 model appears to agree less well with the Jacchia data under such conditions (next subsection).

Our anomalous oxygen data set does not include the high altitude, spin-mode DE-2 neutral mass spectrometer data [Hedin, 1989] for several reasons:

(1) The drag data should account for both O^+ ions and hot O atoms while the DE-2 data account only for the neutral atoms. Therefore, the DE-2 data could bias the fit against the O^+ component detected by the MSX analysis.

(2) Retrieving the hot oxygen component of DE-2 data is dependent on using a model for the cold oxygen component.

(3) The DE-2 data have further limitations: small number of points (425) above 600 km, high solar activity (average $F_{10.7}$ above 190), and narrow temporal coverage (only fall-winter of 1981-2).

Fortunately, a comparison of the Jacchia-Barlier data to the DE-2 data for high latitudes and elevated solar activity (81-day average: $\langle F_{10.7} \rangle > 150$), shows good qualitative agreement, implying that the drag-based data set has captured the elevated neutral density implied by DE-2. A tantalizing result is that the fit of the NRLMSIS anomalous oxygen component to the high-

altitude Jacchia-Barlier total mass density data yielded an effective temperature of approximately 4177 K ± 3 %. We do not hold this to be definitive, given the limitations of our high altitude drag data set, and we have therefore chosen to maintain this parameter at 4000 K, in line with previously cited references on hot oxygen. Note that such a temperature would seem to be too high for oxygen ions to form the primary component of our anomalous oxygen model. Clearly we need more data on, and modeling of, neutral and ionized atomic oxygen at high altitudes to develop a faithful representation of the atmosphere near the exobase.

4.1.2. Comparison of models with high altitude Jacchia data

Comparison of models with the Jacchia data above 600 km reveal both anticipated and unexpected features. First, the high altitude Jacchia data support the observations of Keating et al. [1998], regarding a significant enhancement in total mass density over past MSIS-class models, for the combination of low solar activity, high altitude, and high summer latitudes. However, this difference decreases rapidly with increasing $F_{10.7}$ and decreasing altitude, and surprisingly, the Jacchia-70 model significantly overestimates the observed density at very low $F_{10.7}$. Further, as a function of $F_{10.7}$ under the corresponding winter conditions, MSIS-class models generally agree better with the Jacchia data than does the Jacchia-70 model itself. As a result, NRLMSISE-00 achieves improvements over both MSISE-90 and Jacchia-70, incorporating advantages of each.

Figures 1 and 2 compare the (previous day) $F_{10.7}$ – dependence of the total mass density from four sources: (1) the Jacchia data set on total mass density (data denoted here by ρ_d), (2) the corresponding NRLMSISE-00 model values (ρ_N), (3) the MSISE-90 model values (ρ_M), and (4) the Jacchia-70 model values (ρ_J). The Jacchia-70 model values provide a baseline, since the Jacchia models are the standard of the astrodynamics community for estimating orbital drag. The figures depict bin-averaged differences of natural logarithms, $\log_e(\rho_N/\rho_J)$ denoted by solid lines, $\log_e(\rho_M/\rho_J)$ denoted by dashed lines, and $\log_e(\rho_d/\rho_J)$, located at the centers of the $\pm 1\sigma$ vertical bars (σ = standard deviation). The averaging bins are 10 $F_{10.7}$ units, and both abscissas and ordinates are averages over individual bins. The number at the center of a vertical bar is the approximate base 2 logarithm of the number of points in the corresponding bin. The solid horizontal line at an ordinate of 0.0 represents the bin-averaged Jacchia-70 values. When a vertical bar is approximately centered on the horizontal line, the Jacchia-70 model is in good

agreement with the data in the given bin. Significant displacement of a vertical bar from the horizontal line signifies poor performance by Jacchia-70.

Figure 1(a) shows the solar activity dependence of ρ above 900 km for the combination of summer and high latitudes ($|\theta| \geq 45°$); the MSX data of Keating et al. [1998] correspond to (previous-day) $F_{10.7} = 71$, altitude $z = 900$ km and $\theta = 80.6°$ (N). For low to moderate solar activity (75-175), the Jacchia-70 model captures the trend and magnitude of the data somewhat better than does NRLMSISE-00. A comparison to MSISE-90 verifies the enhancement observed by Keating, but this effect diminishes as $F_{10.7}$ approaches 130. Unexpectedly, as $F_{10.7}$ decreases below 75, the Jacchia-70 model overestimates the total measured mass density by an increasing amount. In fact, below $F_{10.7} \sim 75$, NRLMSISE-00 appears to agree with the Jacchia data better than does Jacchia-70, while above ~ 130 the differences between the two models are relatively small. For the entire data subset containing 684 points, we may also compare the usual statistical measures, i.e., standard deviation, σ, and bias $\beta \equiv \langle \log_e(\rho_d/\rho_{model}) \rangle$, where "model" signifies NRLMSISE-00, MSISE-90, or Jacchia-70, where brackets indicate an average over the data subset, and where the contribution of each datum to both averages has been weighted by the squared reciprocal of the attributed error. The values of (β, σ) are (-0.08, 0.22) for NRLMSISE-00 and (-0.10, 0.24) for Jacchia-70, implying no particular advantage to either model, in spite of the differences in Figure 1(a). MSISE-90 has (β, σ) = (0.19, 0.29), indicating a systematically low average density estimate and a poorer match of the observed $F_{10.7}$ dependence.

Figure 1(b) shows the situation for Jacchia's data set during summer at high latitudes in the altitude range 600-900 km (1085 points). Comparisons with MSISE-90 show that the effect observed by Keating et al. has decreased considerably in both peak value and the operative range of $F_{10.7}$. Moreover, NRLMSISE-00 appears to give better agreement with the dependence of the data on $F_{10.7}$ than does Jacchia-70, and agrees especially well with the data at low solar activity. The statistical measures are (β, σ) = (-0.08, 0.25) for NRLMSIS versus the Jacchia-70 values of (-0.02, 0.31). MSISE-90 has values of (0.05, 0.34), primarily due to poorer agreement at low solar activity. Notice that the bias (β) values of the models are insensitive to the striking differences in variation with $F_{10.7}$ and actually attribute a modest advantage to Jacchia-70, while σ gives a coarse indication that NRLMSISE-00 does a better job matching the F10.7 dependence.

In winter, for the same combination of latitude and altitude, the MSIS-class models generally outperform Jacchia-70 when compared to the Jacchia data set as a function of $F_{10.7}$. Figure 2(a), for $z \geq 900$ km, shows that the Jacchia model gives somewhat better agreement at low $F_{10.7}$ but varies oppositely with the data as $F_{10.7}$ increases. At $F_{10.7} = 98$, the NRLMSIS and MSISE-90 models do show a 45% overestimate, but this is based on only two data points. In fact for $F_{10.7}$ in the range 80 – 120, only 19 data points were available, making the low $F_{10.7}$ range difficult to evaluate. Across the entire range of solar activity, the differences among models show up in the model biases: $(\beta, \sigma) = (-0.06, 0.19)$ for NRLMSISE-00 and (-0.12, 0.20) for MSISE-90 versus the Jacchia-70 values of (-0.24, 0.15).

Figure 2(b), for z = 600-900 km, shows similar but less extreme differences in bias, with $(\beta, \sigma) = (-0.14, 0.19)$ for NRLMSISE-00, (-0.22, 0.21) for MSISE-90 and (-0.20, 0.20) for Jacchia-70. The biases are closer primarily because the number of data points decreased with increasing $F_{10.7}$, for which the deviation of Jacchia-70 from the Jacchia data was also increasing.

The respective β and σ values for NRLMSISE-00 and Jacchia-70 are remarkably similar, especially for the cases in Figure 1, demonstrating that statistical averaging can mask qualitative differences. Such filtering of model estimates by averaging over one or more arguments might explain the comparable performance of MSISE-90 and Jacchia-70 for "special perturbations (SP)" orbit determination [Marcos et al., 1998]. The SP calculation fits a detailed numerical propagator (including drag) to space object observations covering a fit span of several days and acts to filter the density model over the fit span [Neal et al., 1998]. In addition, one of the fitting parameters is the "ballistic coefficient," which multiplies the atmospheric density in the drag term; adjusting the ballistic coefficient corrects the model bias over the fit span [Marcos et al., 1998]. On the other hand, the detailed differences among models play a large role in the important function of orbit prediction, for which no observations of the space object are available.

4.2. Solar ultraviolet occultation vs. mass spectrometry

As indicated above, we have included the UV occultation observations of $[O_2]$ by the Solar Maximum Mission (SMM: [Aikin et al., 1993]) in generating the new model. We have also included UV occultation data derived from a second band (channel 19) on the AE-E EUVS instrument. Prior to NRLMSISE-00, mass spectrometer data were more numerous than were

solar UV occultation data and therefore had a stronger influence on the model profile of $[O_2]$ in the lower thermosphere. Furthermore, the UV occultation data were available only at very low altitudes (≤ 150 km), where comparisons between the two data sources were less definitive [Aikin et al., 1993]. As a consequence, the MSISE-90 profile of $[O_2]$ is in approximate diffusive equilibrium above ~ 150 km [Meier et al, 2001], whereas observations by solar UV occultation differ from diffusive equilibrium by an increasing amount as altitude increases within the range 140-240 km – a longstanding controversy [Aikin et al., 1993, and references therein]. General circulation models and other detailed chemistry/dynamics models also depart from diffusive equilibrium in the lower and middle thermosphere [Meier et al., 2001].

The SMM UV data also show weaker solar activity dependence than do the mass spectrometer data [Aikin et al., 1993]. As a result of these differences, we have modified the parameterization of the lower thermospheric altitude profiles of O_2 and O to allow more flexibility in NRLMSISE-00, as described in the Appendix. The model can now accommodate solar activity dependent departures from diffusive equilibrium in the lower thermosphere. Figure 3(a) shows that the new model compromises between the two data sources in the altitude region 125-225 km covered by the SMM data. Above this region the NRLMSIS $[O_2]$ profile approaches diffusive equilibrium, and below this region, the two data sources agree as the atmosphere approaches a fully mixed state.

Figure 3(b) shows the dichotomy between the newly added data and the previously existing data, from which the MSISE-90 model (horizontal line at 0.0) was generated. The low altitude AE-E UV occultation data (labeled D and E) extended the solar activity dependence of the MSISE-90 database. These data are reasonably consistent with MSISE-90, with mass spectrometer data, and with low altitude, low $F_{10.7}$ AE-C UV occultation data (Figure 3(a) and [Aikin et al., 1993]). On the other hand, the newly added SMM data and the rocket and AE-E UV occultation data at 150 km (labelled K, M, and F and W, respectively) are not generally consistent with the MSISE-90 model, although these data appear to be consistent with each other. Figures 3(a) and (b) show that the magnitude of the disagreement depends on both altitude and $F_{10.7}$, as indicated above.

Figure 3(b) also verifies that the SMM data on $[O_2]$ depend more weakly on $F_{10.7}$ than does MSISE-90, which did not include those data. Figure 3(c) demonstrates that the new

NRLMSISE-00 model fits the $[O_2]$ database far better than MSISE-90, primarily because of the adjustment to the profile in the region of transition from a fully mixed state to diffusive equilibrium.

This leaves open the question of accuracy for both mass spectrometry and solar UV occultation. Before the NRLMSIS models can properly portray the altitude dependence of $[O_2]$, the community must resolve this fundamental conflict of the two major data classes. Note in the Appendix that the [O] profile in the lower thermosphere has also changed to accommodate both the SMM data and the mass spectrometer data on total oxygen number density, $[O] + 2[O_2]$. The latter data are our primary source of information to set the [O] model in NRLMSISE-00. Comparison of the new model with our total oxygen data shows an improvement in standard deviation, but the new model is quite similar to MSISE-90 regarding total oxygen content.

4.3 Exospheric temperature

The Millstone Hill and Arecibo incoherent scatter radar data on exospheric temperature (T_{ex}) are high quality and extend the NRLMSIS database well into the 1990s. These data derive from fitting a model of ion heat balance and chemistry to the ion temperature profile ($T_i(z)$), using ISR observables and parameterized models of neutral oxygen and temperature [e.g., Buonsanto and Pohlman, 1998]. The retrieval of T_{ex} from the ISR data did not include a hot oxygen component [Schoendorf et al. 2000]. The newly added Millstone Hill data, shown in Figure 4(a), cover the period 1981-97. The data include the June, 1991, geomagnetic storm with maximum $\{F_{10.7}, a_p\} \sim \{250, 300\}$ (see Litvin et al. [2000] and references therein) and another period around October 29, 1991 with maximum $\{F_{10.7}, a_p\} \sim \{270, 235\}$. Litvin et al. pointed out that during the most intense storm period of June, 1991, molecular ions dominated the chemistry, requiring a modification in the algorithms used to retrieve T_{ex} ; a similar situation apparently occurred in late October. Even after this correction, however, T_{ex} ranged significantly below the predictions of MSISE-90 for both periods. In fact, given that the difference was greater in October, 1991, when $F_{10.7}$ was higher (Figure 4(a), abscissa ~ 275), the elevated $F_{10.7}$ might also be a factor in the lower value of T_{ex}.

Figure 4(b) shows the variation of the new Arecibo ISR data with previous day $F_{10.7}$; these data also include periods of high geomagnetic activity, with some daily A_p values well over 50. Interestingly, MSISE-90 provides a somewhat better fit at high solar activity (≥ 240) than

does NRLMSISE-00, suggesting that the response to solar forcing might vary with latitude. Unfortunately relatively few data points are available at such high values of $F_{10.7}$ and the database has not supported retrieval of a meaningful latitude-$F_{10.7}$ coupling term. Indeed, no clear advantage for either model emerges from comparison with the entire Arecibo data set on upper thermospheric temperature, which covers the last thirty-five years.

The findings by Millstone Hill under elevated geomagnetic activity in 1991 led naturally to a search for Arecibo measurements that intersected with Millstone Hill data during 1991. Two such periods occurred early in the year (mid-January and mid-March). At those times $F_{10.7}$ was high (180-275) while A_p was low to moderate (< 35). During these periods, the temperature bias relative to NRLMSISE-00 had the same sign at both ISR sites – negative for mid-January with ($F_{10.7}$ ~ 180-220) and positive for mid-March when ($F_{10.7}$ – 240-275). The respective biases were also similar in magnitude, though 20 – 40 % less than the biases during the June and October storm periods. The similarity of biases at the two sites during lower geomagnetic activity points to a global error source in the model; an example is the use of $F_{10.7}$ as a proxy for the solar EUV flux, which drives variability of the thermospheric density on time scales of a day or longer. Bass et al. [1996] and Rhoden et al. [2000], respectively, have used drag and accelerometer data to explore other proxies as candidates to augment or replace $F_{10.7}$. On the other hand, the differing signs of the bias during these lower geomagnetic activity periods contrasts with the decidedly negative bias observed during mid- and late 1991, when maximum a_p was very high.

Most importantly, the new ISR and total mass density data, when combined with the previous MSIS data sets, have changed the solar activity dependence of the temperature in NRLMSISE-00, relative to that of MSISE-90 (and MSIS-86), especially at higher altitudes. Figure 5 shows the difference in mean exospheric temperature estimates produced by the models as a function of latitude and ($F_{10.7}$). The NRLMSISE-00 T_{ex} is above that of MSISE-90 only at low latitudes and for moderate to low ($F_{10.7}$) and then by only a few degrees. As solar activity increases above moderate values, the NRLMSISE-00 value of T_{ex} falls below that of MSISE-90 by a steadily increasing amount, reaching – 40 K at $\langle F_{10.7} \rangle > 220$ and high latitudes, $|\theta| > 45°$. This difference is less pronounced at lower latitudes, as we might expect from Figure 4(b). The mean total mass density behaves similarly to the temperature. Checks of the individual NRLMSISE-00 data sets on composition, temperature, and density have generally confirmed this behavior.

4.4. Mesosphere inversion layers

Mesosphere inversion layers (MIL) are regions of enhanced temperature (ΔT ~ 15-50 K) which have been observed in the upper mesosphere and at the mesopause at low and mid-latitudes and primarily at night [Meriwether and Gardner, 2000]. Present theory attributes the phenomenon to enhancement of tidal structure through interaction with gravity waves; ultimately, a more comprehensive database of 24-hour observations in the mesosphere and lower thermosphere will be needed to confirm and complete the theory. Quantitative analysis of the MIL phenomenon is well beyond the scope of the present paper and the empirical model; here we merely point out NRLMSISE-00 does exhibit the shape of an upper MIL near the mesopause at low latitudes during the nighttime. Under these conditions, this feature is more prominent in the new model than in MSISE-90 and warrants mention. Figure 6(a) shows a comparison of MSISE-90 and NRLMSISE-00 under these conditions while 6(b) shows a similar dayside comparison. The structure becomes less apparent at mid-latitudes, covers a broader altitude range, and appear to be less prominent at midnight than do the annual mean upper MIL profiles shown by Meriwether and Gardner. In this region, the NRLMSIS database contains only a few rocket observations (~ 60 temperature values), which do not appear to have sufficient information to cause this behavior in the model. The figure shows primarily that the formulation is sufficiently flexible to capture MIL structures in data sets. Outside of the addition of new Millstone Hill LTCS data in the 100-130 km altitude range, the only major difference from the MSISE-90 model is the imposition of hydrostatic equilibrium over a wider range (80-300 km). The latter factor plus the lower order tides in the model apparently have acted in concert to produce the MIL-like structure. Generating realistic MIL profiles with NRLMSIS awaits upgrading the model with the recent, extensive database of ground- and space-based observations of the upper mesosphere and mesopause.

5. NRLMSIS Model – Present and Future

The new database underlying the NRLMSISE-00 model incorporates data on total mass density (orbital drag and satellite accelerometers), recent incoherent scatter radar observations covering more than a solar cycle, and satellite-borne FUV occultation measurements of $[O_2]$ from SMM. The model interpolates among newly added and past data sets, often incorporating strengths or features of each data set. As a result, the exospheric temperature in NRLMSISE-00

now shows somewhat weaker dependence on $F_{10.7}$ relative to MSISE-90. In the lower thermosphere, the model compromises between mass spectrometer and ultraviolet occultation data in terms of the altitude dependence of $[O_2]$ but follows the weaker solar activity dependence of UV occultation data more closely.

The incorporation of satellite-based data on total mass density has allowed the inclusion of a new component – "anomalous oxygen" – to correct the model estimates of total density at high altitudes (near the exobase). This recognizes the conclusion of Keating et al. [1998] that O^+ can dominate drag under particular conditions and, through similar analysis, the conclusion of Hedin [1989] that hot oxygen could be important to drag. Comparison of NRLMSIS and the standard operational and scientific models to the orbit-based data of Jacchia at high altitudes has revealed significant differences in the seasonal and solar activity dependence of the models. The new model appears to provide advantages over both Jacchia-70 and MSISE-90 for estimating total mass density.

The broadening of the database, along with comments by users and plans to replace or augment the $F_{10.7}$ input with a superior index of the solar chromospheric extreme ultraviolet (EUV) flux, have led to modifications in the model formulation:

1) A new coupling term between $F_{10.7}$ and mean $F_{10.7}$ (Appendix A.1) to permit more flexibility in representing the dependence on solar EUV.

2) Anomalous oxygen model in upper thermosphere to allow for increased drag under some conditions;

3) Upgraded representation of $[O_2](z)$ in the lower thermosphere to allow more general and higher altitude departures from diffusive non-equilibrium and weaker solar activity dependence [Aikin et al., 1993];

4) New $[O](z)$ parameterization in the lower thermosphere to compensate for changes in the new definition of $[O_2](z)$, primarily when fitting mass spectrometer data on total oxygen content, $[O] + 2[O_2]$;

5) Hydrostatic equilibrium constraint over a wider altitude range to tie the upper and lower atmospheric regions together self-consistently;

6) Nonzero thermal diffusion factor for Ar.

Item (5) is particularly interesting, in that NRLMSISE-00 produces a temperature structure similar to a mesosphere inversion layer under some conditions (e.g., equatorial region at night, low latitudes), even though our most proximate new temperature data are above the mesopause (altitude range 100-130 km [Goncharenko and Salah, 1998]). We attribute this effect to the self-consistent imposition of hydrostatic equilibrium across the mesopause, in combination with the interaction among low order tides. Presumably the next generation NRLMSIS model will provide a more accurate climatology of the MIL when the relevant satellite- and ground-based data are added to the database.

An underlying theme of this paper and of our future work is the dependence of the upper atmosphere on the solar EUV flux, which is the primary driver on time scales of a day or longer. Section 4 shows that the dependence on the $F_{10.7}$ solar EUV proxy is different for the respective empirical models favored by operational and scientific communities. The new NRLMSISE-00 model appears to incorporate advantages of both model classes and therefore helps to close the gap between these models. In addition, the atmospheric calibration method of Marcos et al. [1998] and a follow-on implementation in terms of ultraviolet remote sensing use near-real-time atmospheric data to improve density estimation for the "present" epoch [Nicholas et al., 2000]. Ultimately, however, the operational community seeks a better predictive capability. Marcos et al. [1998] have shown that the most likely route to this goal is through better solar EUV inputs to the models, such as that by Lean et al. [2001]. Under funding by the NASA Living With a Star Program, we are now pursuing this approach.

Acknowledgements

The authors gratefully acknowledge primary support by the Office of Naval Research, early support for one of us (A. Hedin) by the NASA Supporting Research & Technology Program, and recent support by the NASA Living With a Star Program. Generously providing new data sets and vital assistance to us were the following: Frank Marcos (AFRL: accelerometer data); Francois Barlier (drag data, including those of Jacchia); Steven Cariglia, John Holt, Joseph Salah, and Michael Buonsanto (Millstone Hill, MIT Haystack Observatory: T_{ex}); Joseph Salah and Larisa Goncharenko (Millstone Hill, MIT Haystack Observatory: Lower Thermosphere Coupling Study, $T_{100\text{-}130}$); and Michael Sulzer and the CEDAR Database (Arecibo: T_{ex}). Millstone Hill, through its staff members John Holt, Michael Buonsanto, and Steven Cariglia,

kindly invited and trained our research associate Owen Kelley, who retrieved T_{ex} from both the Millstone Hill and the Arecibo data sets in the Madrigal Database. The data provided by the Millstone Hill incoherent scatter radar were obtained under a National Science Foundation cooperative agreement with MIT, ATM-9714593. Robert Meier performed extensive testing of the new model in spectral inversion and data-fitting codes, and John Mariska and John Holt tested the distribution package on a number of operating systems. We have also received invaluable guidance from William Oliver, Daniel Melendez-Alvira, Raymond Roble, and Anatoli Pavlov.

Appendix: NRLMSISE-00 formulation, constraints, generation, and distribution package

A.1. Formulation

The Appendix of Hedin [1987] defines the thermospheric portion of the MSIS-class models, for which the fundamental variable is the temperature T(z). The Bates-Walker temperature profile variables [Walker, 1965] are the exospheric temperature, T_{ex} ; the temperature at 120 km, T_{120}; and the temperature gradient at $z_{lb} \equiv 120$ km. These variables have the form (e.g., for T_{120})

$$T_{120} = \bar{T}_{120}[1 + G_{120}(L)] \ ,$$

where the overbar signifies a global and temporal mean and the function G(L) includes constant, spherical harmonic, and harmonic terms, some of which are coupled and whose coefficients and phases represent the spatial and temporal time scales inherent in the data. In addition, G(L) contains polynomial or exponential terms in the solar EUV proxy ($F_{10.7}$ and $\langle F_{10.7} \rangle$, the 81-day average) and in geomagnetic activity. For chemical species i, the Bates-Walker profile variable is the number density at 120 km

$$n_i = \bar{n}_i \exp\left[G_i(L)\right] \ .$$

The subscript on G distinguishes among unique coefficient sets for respective thermospheric variables in the model. The Bates-Walker profile represents species in thermal and diffusive equilibrium and includes thermal diffusion. Below a species-dependent altitude in the range 160-450 km, the model profiles differ from diffusive equilibrium by progressively greater amounts as z decreases, transitioning to a fully-mixed state at a turbopause $z_h \sim 100$ km. In that region,

MSIS-class models modify the density profile due to the effects of chemistry, dynamics, and loss and flow processes.

The NRLMSISE-00 model incorporates the following modifications of the equations in Hedin [1987]:

(1) The solar EUV dependence includes a new cross term with coefficient $B \neq 0$:

$$G(\text{Solar}) = A\,\Delta F\,(1+B\,\Delta\langle F\rangle) + C\,(\Delta F)^2 + D\,\Delta\langle F\rangle + E\,(\Delta\langle F\rangle)^2,$$

where $\langle F_{10.7}\rangle$ is the 81-day, time-centered average of $F_{10.7}$, $\Delta\langle F\rangle = \langle F_{10.7}\rangle - 150$, and $\Delta F = F_{10.7} - \langle F_{10.7}\rangle$.

(2) The "anomalous" oxygen model profile, $[O_a](z)$, represents nonthermal oxygen species (e.g., O^+ and hot oxygen) inherent in the Jacchia and Barlier data sets at higher altitudes (≥ 600 km) and is similar to an ionospheric Chapman layer (e.g., Cotton et al., [1994]),

$$[O_a](z) = [O_a](z_{lb}) \exp\left\{-\frac{\xi(z, z_{lb})}{H(z_{lb}, T_a)}\right\} \exp\left\{\frac{C}{H(z_a, T_a)}\left[1 - \exp\left(-\frac{z - z_a}{C}\right)\right]\right\},$$

where the geopotential height is $\xi(z, z_{lb}) = z - z_{lb}$, the scale height is $H(z, T) \equiv \dfrac{kT}{mg(z)}$, m is the mass of atomic oxygen, and the constants are $C = 76$ km, $z_a = 550$ km, $T_a = 4000$ K, $z_{lb} = 120$ km, and $[O_a](z_{lb})$ (set by data) $= 6.0 \times 10^4$ cm^{-3}.

(3) Equations (A20a) and (A20b) of Hedin [1987] define a lower thermospheric density multiplier C_1 in Equation (A12a); the purpose of this factor is to simulate chemistry and dynamic flow effects on various species. For [O] and $[O_2]$ this factor now takes the form

$$C_1 = \exp\left\{\frac{R}{1 + \exp\left[(z - z_c)/H_c\right]}\right\},$$

where $R = R_i\,(1 + a_f\,\Delta\langle F\rangle)$ and $i = O, O_2$. The constants are $R_O = -0.045$, $R_{O_2} = -0.78$, $a_f = 0.029$, $H_c(O) = -H_c(O_2) = 21.2$ km (Note: opposite signs), and $z_c(O) = z_c(O_2) = 129.4$ km.

(4) Consistent with Banks and Kockarts [1973], the thermal diffusion factors in NRLMSISE-00 are $\alpha_i = -0.38$ (i = He, H), 0.17 (i = Ar), 0.0 (other species). This represents a change from MSISE-90, which had $\alpha_i = -0.4$ (i = He, H) and 0.0 (other species). Pavlov [1979] and (private

communication, 1998) suggests the following values: -0.38 (H), -0.28 (H_2), -0.27 (He), 0.17 (Ar), 0.12(O_2), -0.08 (O), and 0.1 (N_2).

A.2. Constraints

For altitudes $0 \leq z < z_{lb} \sim 120$ km, the fundamental variables define nodes and gradients of the temperature profile, while pressure and density are defined by hydrostatic equilibrium and the ideal gas law [Hedin, 1991]. As mentioned above, diffusive equilibrium no longer holds for the MSIS-class models below altitudes ~ 300 km. Because we fit the temperature and individual species separately (different coefficient sets), the MSIS-class models do not maintain hydrostatic equilibrium *a priori*. For this reason, the model generation process imposes an approximate hydrostatic equilibrium constraint in the region 80 - 300 km. This couples the lower and upper atmospheric regions, modifying some details of previous MSIS versions. Finally, since the new data all relate to the thermosphere, NRLMSISE-00 retained the MSISE-90 coefficients below while constraining coefficient values in the range 72.5 - 110 km to give a total mass density at the ground in agreement with MSISE-90.

A.3. Model generation

Generating a new version of the model requires calculation of optimal values for the ~ 2200 nonzero coefficients. Even though only a subset of the MSIS database is used to evaluate [Hedin et al., 1977], the number of data points is still quite sizable (~ 3×10^5), rendering an inclusive Levenberg-Marquardt calculation [Press et al., 1992] compute-intensive and cumbersome. Because the NRLMSIS thermospheric data are separable by mass number (species, temperature, total mass density), one can partition the process into a series of separate Levenberg-Marquardt (LM) χ^2 minimization calculations for coefficient and data subsets for different altitude regions, magnetic activity level, and scales of variability. Each complete series of LM coefficient calculations (presently numbering fifty-two) constitutes one "grand" fitting cycle. The grand cycles repeat until the coefficient set is stable [Hedin, 1987]. This approach has minimized memory requirements and maximized computing speed. We eliminate severe outliers by selecting only data points whose residuals are less than a specified multiple (6-15) of the observational uncertainty.

The new drag and accelerometer data represent a significant departure from the above picture. In the present case, the total mass density provided by the model is a secondary or inferred quantity, given by the sum of species mass densities, apparently requiring that all of the species coefficients vary simultaneously to fit the data, which are extensive. To avoid this and other procedural difficulties, one can take advantage of the fact that different thermospheric species dominate the mass density in different altitude regions. Specifically, for N_2, O_2, and He, we have used the MSISE-90 model to determine the altitude ranges where the respective mass fractions are greater than 50 %, thereby splitting the data into subsets. We have added these data subsets to the databases supporting the individual species coefficients and have combined the calculations of coefficients for N_2 and exospheric temperature (T_{ex}). As described in Section 4.1, we have extracted the high altitude (≥ 600 km) Jacchia and Barlier data to compute the coefficients associated with anomalous oxygen species and have excluded the summer-high-altitude Jacchia and Barlier data in determining the standard thermospheric constituents.

A.4. Distribution Package and Access

The present NRLMSISE-00 distribution package is an ASCII file containing the model source, a test driver, and the expected output of the test driver. Users may acquire the file via two methods:

(1) download from our website: http://uap-www.nrl.navy.mil/models_web/msis/msis_home.htm

(2) send e-mail to NRLMSISE-00@uap2.nrl.navy.mil (no subject or message), which will result in a reply with the file as an attachment.

References

Aikin, A. C., Hedin, A. E., Kendig, D. J., and Drake, S., Thermospheric Molecular Oxygen Measurements Using the Ultraviolet Spectrometer on the Solar Maximum Mission Spacecraft, *J. Geophys. Res., 98*, 17607-13, 1993.

Arduini, C., U. Ponzi, G. Laneve, "Tidal Analysis of the San Marco V and San Marco III: Density Data in Equatorial Orbit," *J. Atmos. Solar-Terr. Phys., 59 (13)*, 1491-1503, 1997.

Banks, P. M. and Kockarts, G., *Aeronomy, Part B*, Academic Press, New York, 1973.

Bass, J. N., M. J. Kendra, J. M. Griffin, D. R. Larson, N. Ericson, and T. Killeen, Computer Efficient Models of Thermospheric Density and Composition: Application of Satellite Data in Near Real Time – Final Report, Report No., PL-TR-96-2150, (Phillips Laboratory, Hanscom AFB, MA, 1996).

Barlier, F., Berger, C., Falin, J. L., Kockarts, G., and Thuillier, G., A thermospheric model based on satellite drag data, *Ann. Geophys., 34*, 9-24, 1978.

Boudon, Y., F. Barlier, A. Bernard, R. Juillerat, A. Mainguy, "Synthesis of Flight Results of the CACTUS Accelerometer for Accelerations Below 10-9g," *Acta Astronaut, 6 (11)* 1387-1398, 1979.

Buonsanto, M. J., and Pohlman, L. M., Climatology of neutral exospheric temperature above Millstone Hill, *J. Geophys. Res., 103*, 23381-23392, 1998.

Champion, K. S. W., and F. A. Marcos, "The Triaxial-Accelerometer System on Atmosphere Explorer," *Radio Science, 8(4)*, 297-303, 1973.

Cotton, D. M., G. R. Gladstone, and S. Chakrabarti, Sounding Rocket Observation of a Hot Atomic Oxygen Geocorona, *J. Geophys. Res, 98*, 21651-7, 1994.

Goncharenko, L. P. and Salah, J. E., Climatology and variability of the semidiurnal tide in the lower thermosphere over Millstone Hill, *J. Geophys. Res., 103*, 20715-20726, 1998.

Gonzalez, S. A., and M. P. Sulzer, Detection of He^+ Layering in the Topside Ionosphere Over Arecibo During Equinox Solar Minimum Conditions, *Geophys. Res. Lett., 23(18)*, 2509-12,1996.

Hedin, A. E., Extension of the MSIS thermosphere model into the middle and lower atmosphere, *J. Geophys. Res., 96*, 1159-1172, 1991.

Hedin, A. E., Hot oxygen geocorona as inferred from neutral exospheric models and mass spectrometer measurements, *J. Geophys. Res., 94*, 5523-5529, 1989.

Hedin, A. E., High altitude atmospheric modeling, *NASA Tech. Memo. 100707*, 1988.

Hedin, A. E., MSIS-86 thermospheric model, *J. Geophys. Res., 92*, 4649-4662, 1987.

Hedin, A. E., J. E. Salah, J. V. Evans, C. A. Reber, G. P. Newton, N. W. Spencer, D. C. Kayser, D. Alcayde, P. Bauer, L. Cogger, and J. P. McClure, A Global Thermospheric Model

Based on Mass Spectrometer and Incoherent Scatter Data MSIS 1. N2 Density and Temperature, J. Geophys. Res., 82 (16), 2139-2147, 1977.

Jacchia, L., New Static Models of the Thermosphere and Exosphere with Empirical Temperature Profiles," *Smithsonian Astrophys. Observatory Special Rep. No. 313*, May 6, 1970.

Kayser, D. C., Solar flux variation of the thermospheric molecular oxygen density, *J. Geophys. Res., 85*, 695-702, 1980.

Keating, G. M., Leary, J. C., Green, B. D., Uy, O. M., Benson, R. C., Erlandson, R. E., Phillips, T. E., Lesho, J. C., and Boies, M. T., Neutral and ion drag effects near the exobase: MSX satellite measurements of He and O^+, *AAS 97-634* and in *Astrodynamics 1997, Adv. Astronaut. Sci., Part 1, 97*, ed. by F. Hoots, B. Kaufman, P. Cefola, and D. Spencer, Amer. Astronaut. Soc., San Diego, 549-556, 1998.

Knowles, S. H., J.M. Picone, S. Thonnard, A. Nicholas, The Effect of Atmospheric Drag on Satellite Orbits During the Bastille Day Event, *Solar Physics*, submitted, 2001.

Lean, J. L., O. R. White, W. C. Livingston, and J. M. Picone, "Variability of a Composite Chromospheric Irradiance Index During the 11-Year Activity Cycle and Over Longer Time Periods," *J. Geophys. Res., 106 (A6)*, 10645-58 (2001).

Litvin, A., W. L. Oliver, J. M. Picone, M. J. Buonsanto, The upper atmosphere during 5-11 June 1991," J. Geophys. Res. 105(A6), 12789-96 (2000).

Marcos, F. A., Hedin, A. E., Liu, J., Bass, J. N., and Baker, C. R., Operational satellite drag model standards, *AIAA 95-0551, 33rd Aerospace Sciences Meeting & Exhibit, Reno, NV*, 1995.

Marcos, F. A., M. J. Kendra, J. M. Griffin, J. N. Bass, D. R. Larson, and J. J. F. Liu, "Precision Low Earth Orbit Determination Using Atmospheric Density Calibration," *AAS 97-631*, and in *Astrodynamics 1997: Advances in the Astronautical Sciences, Vol. 97(1)*, ed. by F. Hoots, B. Kaufman, P. Cefola, and D. Spencer, Am. Astronaut. Soc., San Diego, 501-513, 1998.

Meriwether, J. W., and C. S. Gardner, A review of the mesosphere inversion layer phenomenon, J. Geophys. Res., 105(D10), 12405-16, May 27, 2000.

Melendez-Alvira, D. J., Picone, J. M., Kelley, O. A., Zhou, Q., and Sulzer, M. P., Histograms of Arecibo World Days measurements and linear-H fits between 1985 and 1995, *NRL Memo. Rep. NRL/MR/7640-98-831*, 1998.

Meier, R. R., J. M. Picone, D. P. Drob, and R. G. Roble, Similarity Transformation-Based Analysis of Atmospheric Models, Data, and Inverse Remote Sensing Algorithms, *J. Geophys. Res.*, to be published (2001).

Neal, H. L., S. L. Coffey, and S. Knowles, "Maintaining the Space Object Catalog with Special Perturbations," *AAS 97-687*, and in *Astrodynamics 1997: Advances in the Astronautical Sciences, Vol. 97(2)*, ed. by F. Hoots, B. Kaufman, P. Cefola, and D. Spencer, Am. Astronaut. Soc., San Diego, 1349-60, 1998.

Nicholas, A., J. M. Picone, S. E. Thonnard, R. R. Meier, K. F. Dymond, and D. P. Drob, "A Methodology for using Optimal MSIS Parameters Retrieved from SSULI Data to compute Satellite Drag on LEO Objects," *J. Atmos. Solar-Terr. Phys. 62*, 1317-26, 2000.

Oliver, W. L., Hot oxygen and the ion energy budget, *J. Geophys. Res., 102(A2)*, 2503-11, 1997.

Oliver, W. L., and J. Schoendorf, Variations of hot O in the thermosphere, *Geophy. Res. Lett., 26(18)*, 2829-32, 1999.

Pavlov, A. V., Thermal Diffusion in the Upper Atmosphere of the Earth, *Geomagnetism and Aeronomy, 19(6)*, 707-11 (1979).

Press, W. H., Teukolsky, S. A., Vetterling, W. T., and Flannery, B. P., *Numerical Recipes: The Art of Scientific Computing*, Cambridge University Press, New York, 1992.

Rhoden, E. A., J. M. Forbes, and F. A. Marcos, The influence of geomagnetic and solar variabilities on lower thermosphere density, *J. Atmos. Solar-Terr. Phys. 62*, 999-1013, 2000.

Schoendorf, J., L. A. Young, and W. L. Oliver, Hot oxygen profiles for incoherent scatter radar analysis of ion energy balance, *J. Geophys. Res., 105(A6)*, 12823-12832, June 1, 2000.

U.S. Standard Atmosphere, 1976, U.S. Government Printing Office, Washington, D.C., 1976.

Walker, J. C. G., Analytic Representation of Upper Atmosphere Densities Based on Jacchia's Static Diffusion Models, *J. Atmos. Sci., 22*, 462-3 (1965).

Yee, J. H., J. W. Meriwether, Jr., and P. B. Hays, Detection of a Corona of Fast Oxygen Atoms during Solar Maximum, *J. Geophys. Res., 85(A7)*, 3396-3400, July 1, 1980.

Figures

Might want to add something about ±σ bars in here in case talking about in text.

1. Natural logarithm of total mass density (data and model values) vs. previous-day $F_{10.7}$ for the combination of summer, high latitudes, and high altitudes: (a) $z \geq 900$ km and (b) 600 km $\leq z \leq 900$ km. The density values are normalized to the Jacchia-70 model and are averaged in bins of 10 $F_{10.7}$ units. Vertical bars correspond to the $\pm 1\sigma$ range of Jacchia data within each bin; the Jacchia-70 model values fall on the horizontal line at 0.0. NRLMSISE-00 corresponds to the solid curve and MSISE-90 to the dashed curve.
2. Same as Figure 1 for the combination of winter, high latitudes, and high altitudes: (a) $z \geq$ 900 km and (b) 600 km $\leq z \leq$ 900 km.
3. (a) Lower thermospheric profile of $[O_2]$: $\log_e$ of ratio to MSISE-90 values. Averaging interval: 2 km. Solid curve: NRLMSISE-00 values. Letters and symbols identify individual data sources (Acronyms: Atmospheric Explorer missions, AE; Solar Maximum Mission, SMM) – Solar Ultraviolet Occultation: (K) SMM, (A) AE-C, 100 km, (B) AE-C, 130 km, (V) AE-C, 150 km, (D) AE-E, 100 km, (E) AE-E, 130 km, (F) AE-E, 150 km, channel 19, (W) AE-E, 150 km, channel 06, (M) Rocket; Mass Spectrometer: (C) AE-C, (G) AE-D, (J) AE-E, (+) Rocket.
   (b) Natural logarithm of lower thermospheric $[O_2]$ vs. mean $F_{10.7}$, averaged within bins of 10 flux units. The plot shows the mean of data values normalized by MSISE-90. Vertical bars correspond to the $\pm 1\sigma$ range of normalized $[O_2]$ values within each bin. MSISE-90 corresponds to the horizontal line at 0.0.
   (c) Same as (b), but with data normalized to NRLMSISE-00, which corresponds to the horizontal line at 0.0.
4. T_{ex} vs. $F_{10.7}$ (previous day), averaged over bins of 10 flux units: (a) Millstone Hill data (1981-97) and (b) Arecibo data (1985-95). The quantities plotted are, respectively, differences of data (vertical bars) and of NRLMSISE-00 model values (solid curve) from MSISE-90 (horizontal line at 0.0).
5. Exospheric temperature difference between NRLMSISE-00 and MSISE-90, averaged over longitude and time, as a function of latitude and $\langle F_{10.7} \rangle$.

6. Examples of temperature profiles resembling mesosphere inversion layers, produced by NRLMSISE-00 (solid curve) and MSISE-90 (dashed curve). Conditions: (a) local time 2100 hr and (b) local time 1000 hr, both at 0 UT, day 90, latitude 5°, longitude 315°, $F_{10.7} = \langle F_{10.7} \rangle = 150$, $A_p = 4$.

Introduction to tables in AGU Electronic Dataset Archive:

Tables of Empirical Model Comparisons with the NRLMSIS Database

The following tables compare all data sets in the NRLMSIS database to the corresponding values of several empirical models: NRLMSISE-00 (M00), MSISE-90 (M90), and Jacchia-70 (J70). The tables provide values of the bias or mean residual ("MEAN") and standard deviation ("SD") as functions of geomagnetic activity (quiet, high, and all levels). The tables include both the model generation database and the complete, newly added data sets (designated by footnotes). For temperature T, the tables show a mean residual $\equiv \langle T_i(\text{data}) - T_i(\text{model}) \rangle$ and $\sigma \equiv (([T_i(\text{data}) - T_i(\text{model})]^2) - \beta^2)^{1/2}$ in units of Kelvin. For species number density and total mass density, we have expressed the mean residual as an average fractional density bias $\beta = \exp(\log_e(\rho_i(\text{data})/\rho_i(\text{model})) - 1$, and have computed the standard deviation as $\sigma = ((\log_e^2\{\rho_i(\text{data})/\rho_i(\text{model})\}) - \beta^2)^{1/2}$.

The accompanying paper, "NRLMSISE-00 Empirical Model of the Atmosphere: Statistical Comparisons and Scientific Issues," (J. M. Picone, A. E. Hedin, D. P. Drob, and A. C. Aikin, J. Geophys. Res. xxx, 200x), and references therein provide background on the data sets. Accompanying the data set same is a descriptor; abbreviations include "accel" (accelerometer), "drag" (drag from orbit determination), "NMS" (neutral mass spectrometer), "IMS" (ion mass spectrometer), "ISR" (incoherent scatter radar), and "UV occ" (solar ultraviolet occultation).

Figures 1-2

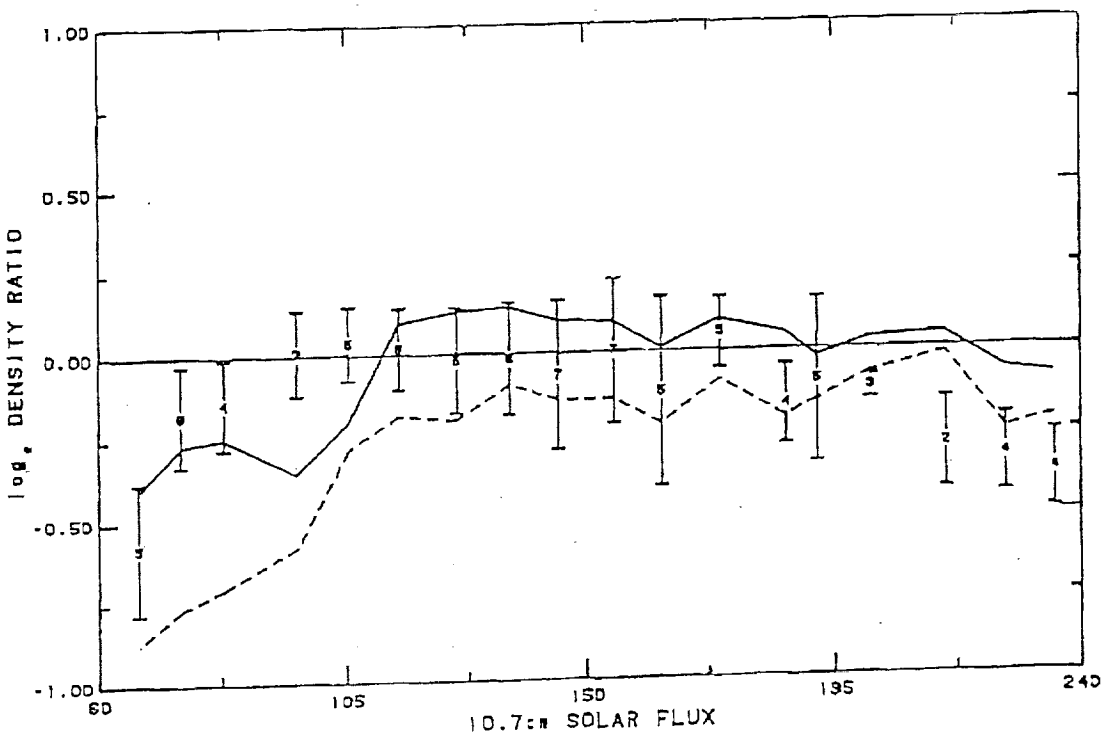

Figure 1(a)

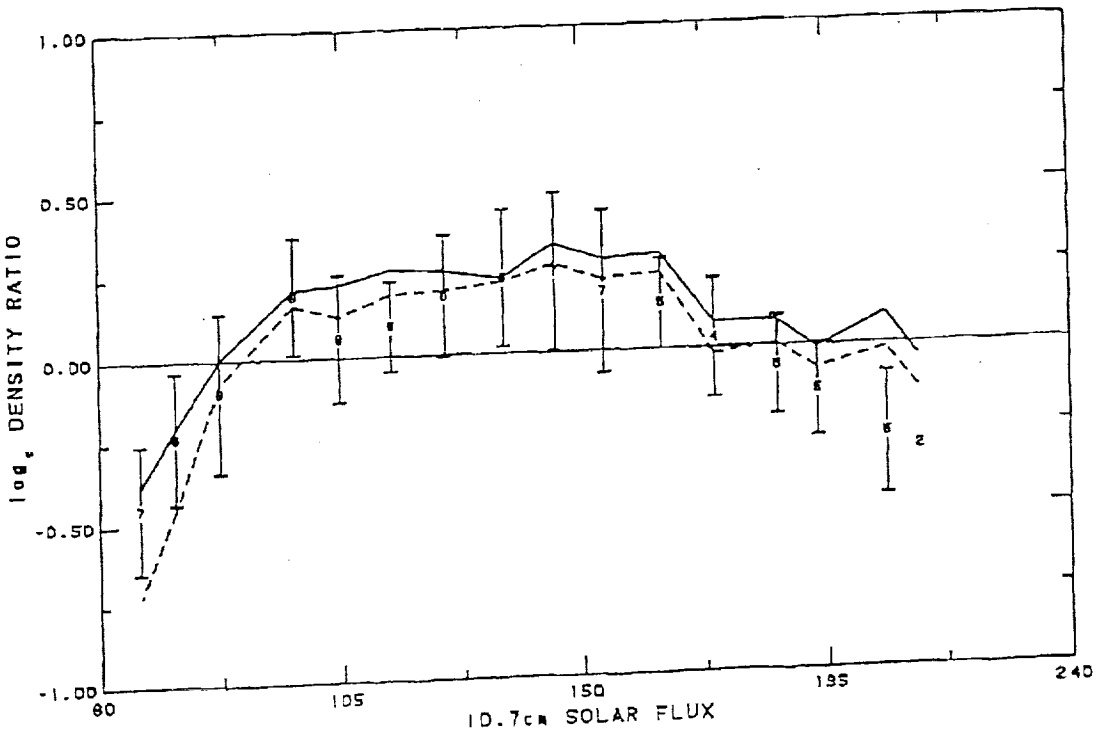
1.00
0.50
0.00
-0.50
-1.00
log$_e$ DENSITY RATIO
80
105
150
195
240
10.7cm SOLAR FLUX

Figure 1(b)

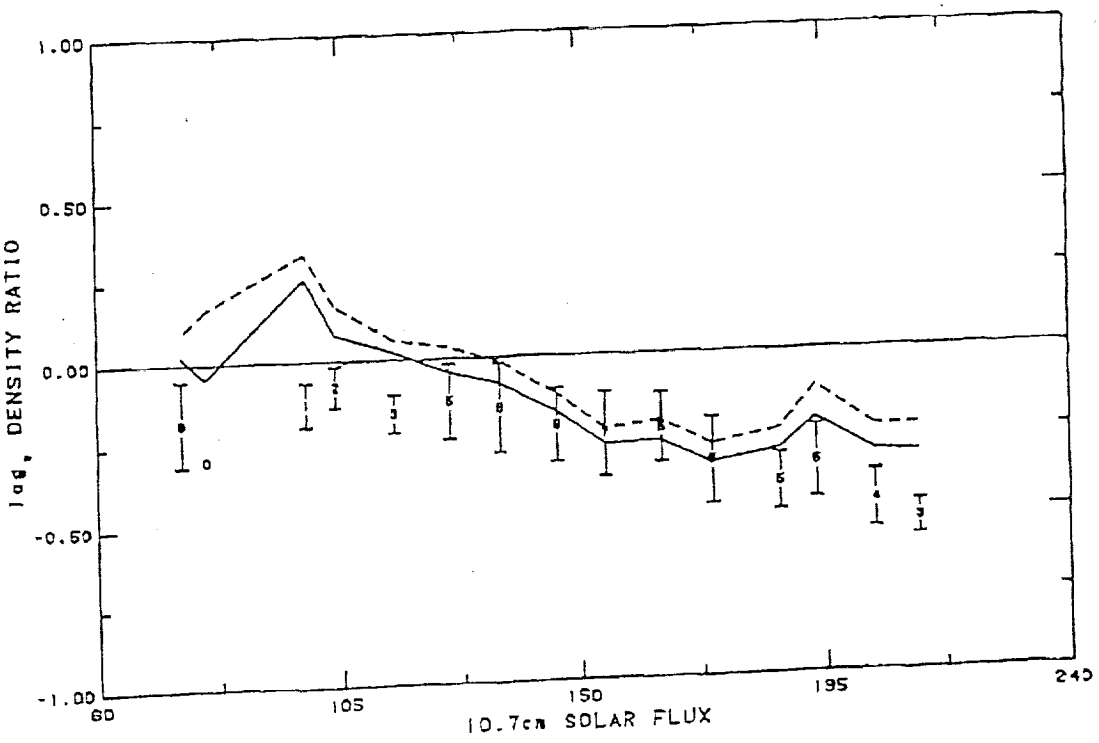
1.00
0.50
0.00
-0.50
-1.00
log$_e$ DENSITY RATIO
60
105
150
195
240
10.7cm SOLAR FLUX

Figure 2(3)

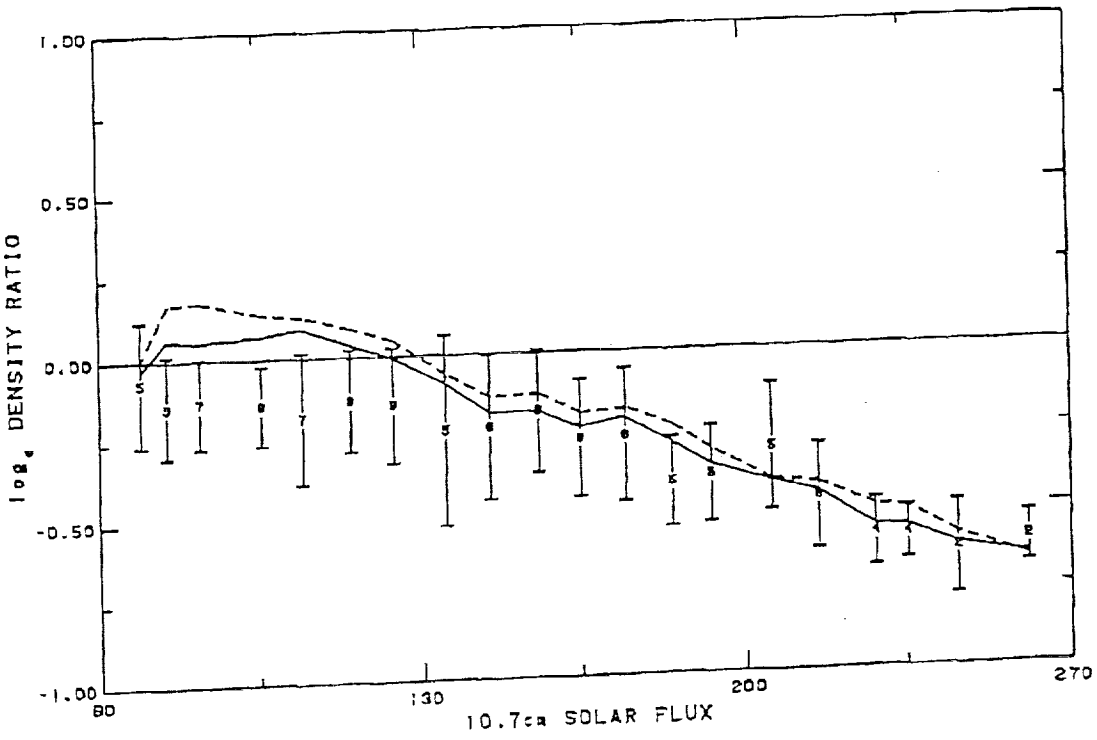
1.00
0.50
0.00
-0.50
-1.00
log DENSITY RATIO
80
130
200
270
10.7cm SOLAR FLUX

Figure 2(b)

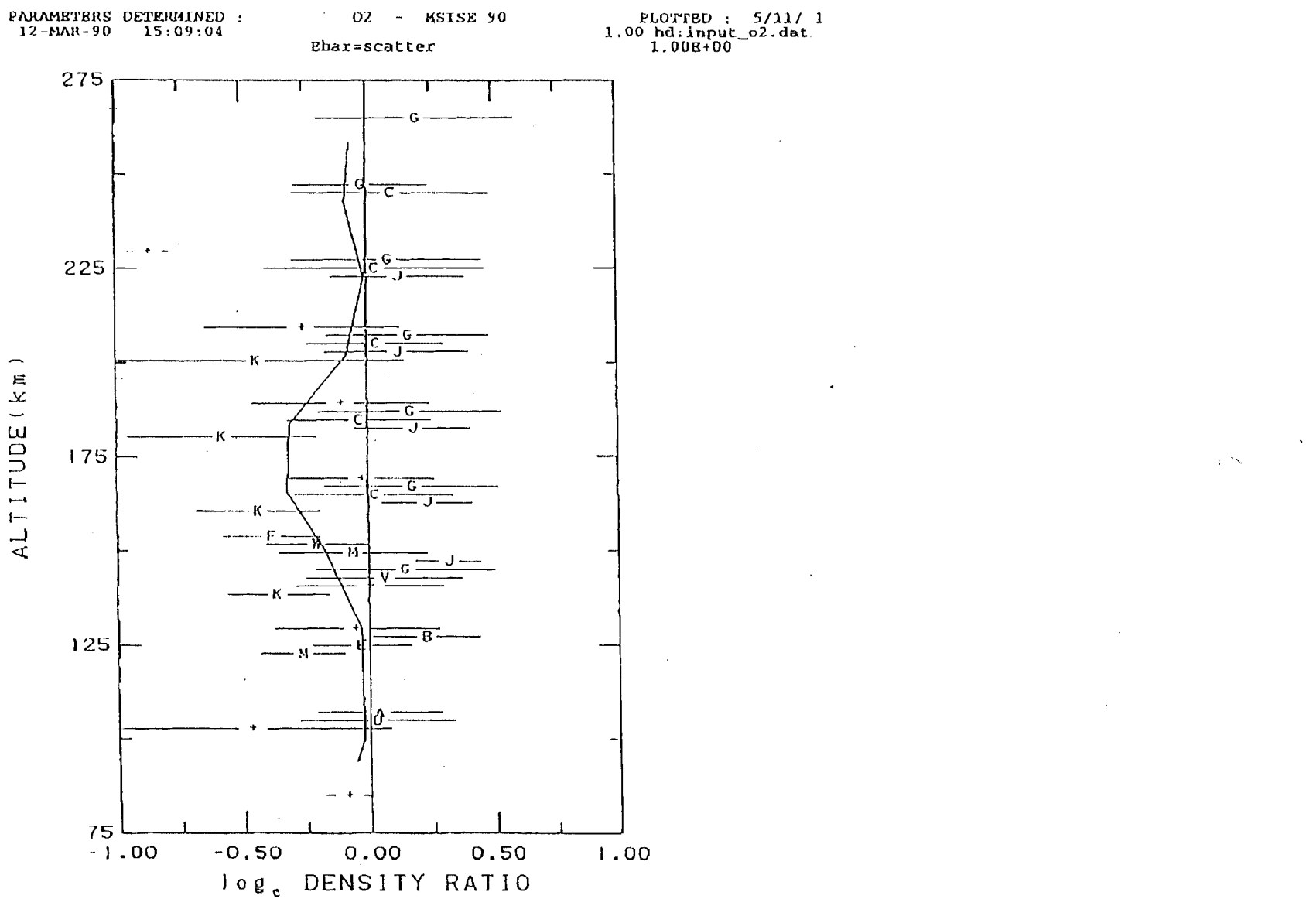
PARAMETERS DETERMINED : O2 - MSISE 90 PLOTTED : 5/11/ 1
12-MAR-90 15:09:04 1.00 hd:input_o2.dat
Ebar=scatter 1.00E+00
275
225
175
125
75
ALTITUDE (KM)
-1.00
-0.50
0.00
0.50
1.00
log e DENSITY RATIO
NS 32 GRP: 0 ALTL: -1.,1201.ISK: 39, 15. SEL: 0 0.0 0.0 PTS PLT: 4675 AVG: -0.22 SD: 0.41 A: 2.000 20.000
KP 0 SW: 1. 1. 1. 1. 1. 1. 1. 1.-1. 1. 1. 1. 1. 1. D1,D2: 61235 89321 ST,SX,SY 0 0 0 SM 1.00 DATA&MODEL 3 G
AVG,SD -0.0735 0.1496 AVXL,AVXH 0. 0. RMS 0.4632 DSD,MSD,R 4.1315 4.1352 1.00 KDM 4 ZANM 0
F 0.00(0.0) 0.00(0.0) 0.00(0.0) B 0.000(0.0) 0.000(0.0) 0.000(0.0) M 0.00(0.0) 0.00(0.0) 0.00(0.0)ABX*****

Fig 3(a)

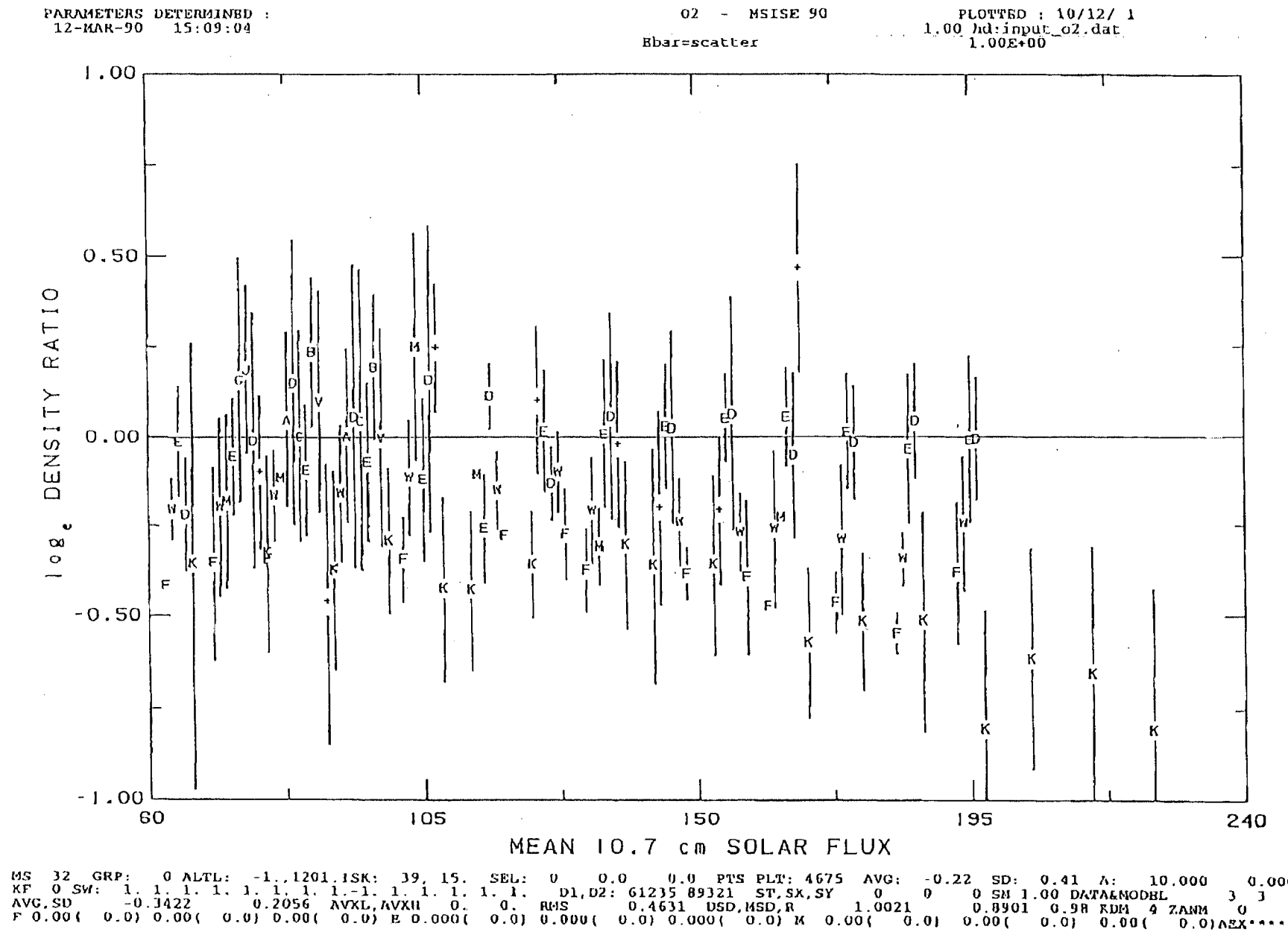

MS 32 GRP: 0 ALTL: -1.,1201.ISK: 39, 15. SEL: 0 0.0 0.0 PTS PLT: 4675 AVG: -0.22 SD: 0.41 A: 10.000 0.000
KP 0 SW: 1. 1. 1. 1. 1. 1. 1. 1.-1. 1. 1. 1. 1. 1. D1,D2: 61235 89321 ST,SX,SY 0 0 0 SN 1.00 DATA&MODEL 3 3
AVG,SD -0.3422 0.2056 AVXL,AVXH 0. 0. RMS 0.4631 USD,MSD,R 1.0021 0.8901 0.98 RDM 4 ZANM 0
F 0.00(0.0) 0.00(0.0) 0.00(0.0) E 0.000(0.0) 0.000(0.0) 0.000(0.0) K 0.00(0.0) 0.00(0.0) 0.00(0.0)AEX****

Fig. 3(6)

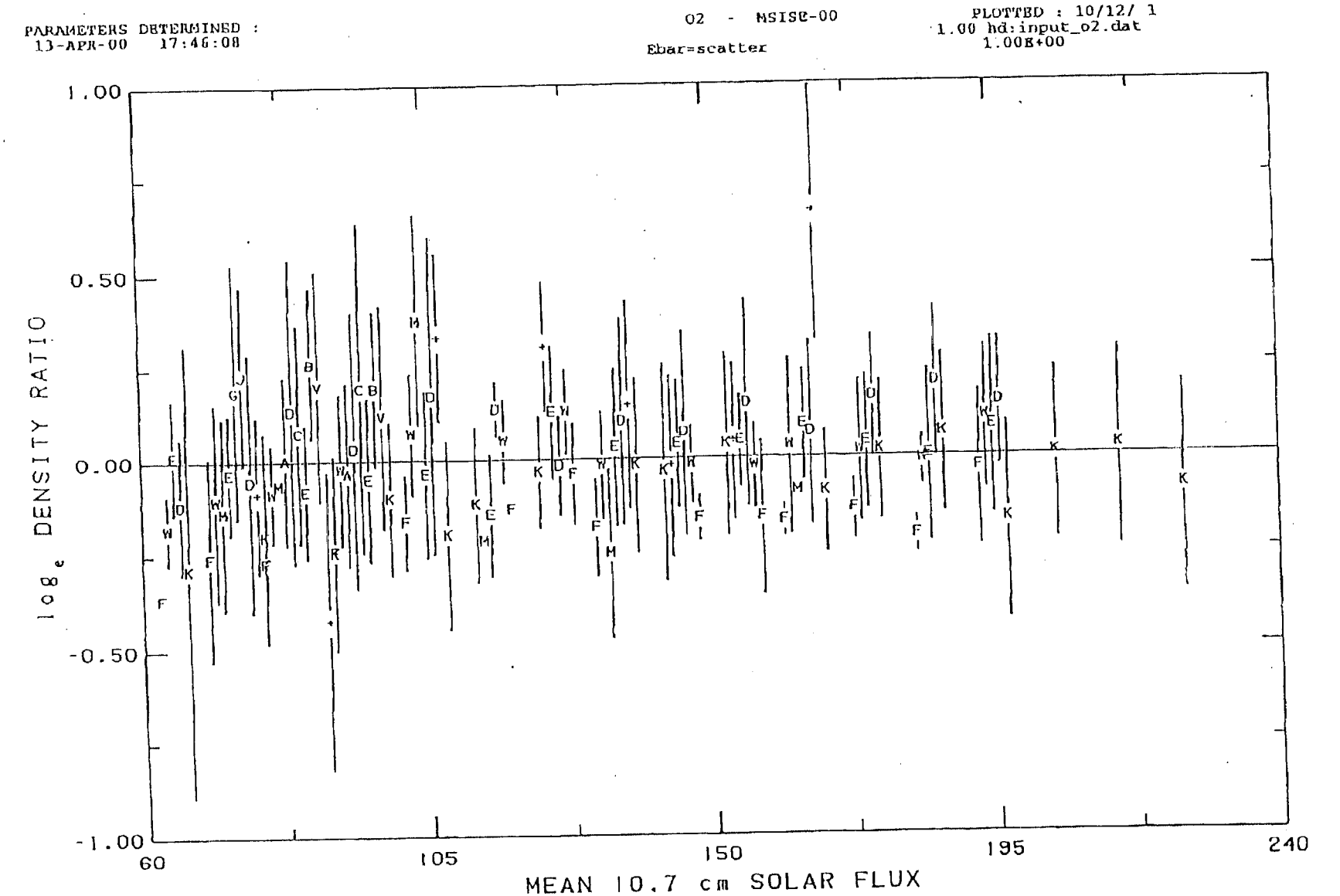

MS 32 GRP: 0 ALTL: -1.,1201,ISK: 39, 15. SEL: 0 0.0 0.0 PTS PLT: 4675 AVG: 0.00 SD: 0.30 A: 10.000 0.000
KP 0 SW: 1. 1. 1. 1. 1. 1. 1. 1. 1.-1. 1. 1. 1. 1. 1. D1,D2: 61235 89321 ST,SX,SY 0 0 0 SM 1.00 DATA&MODEL 6 6
AVG,SD -0.0281 0.0652 AVXL,AVXI 0. 0. RMS 0.3016 DSD,MSD,R 1.0021 1.0017 1.00 KDN 4 ZANM 0
F 0.00(0.0) 0.00(0.0) 0.00(0.0) E 0.000(0.0) 0.000(0.0) 0.000(0.0) M 0.00(0.0) 0.00(0.0) 0.00(0.0)AEX****

Fig. 3(c)

PARAMETERS DETERMINED :
12-MAR-90 15:09:04

TEMP - MSISE 90
Rbar=scatter

PLOTTED : 5/14/ 1
1.00 hd:mlhtex8197.dat
1.00E+00

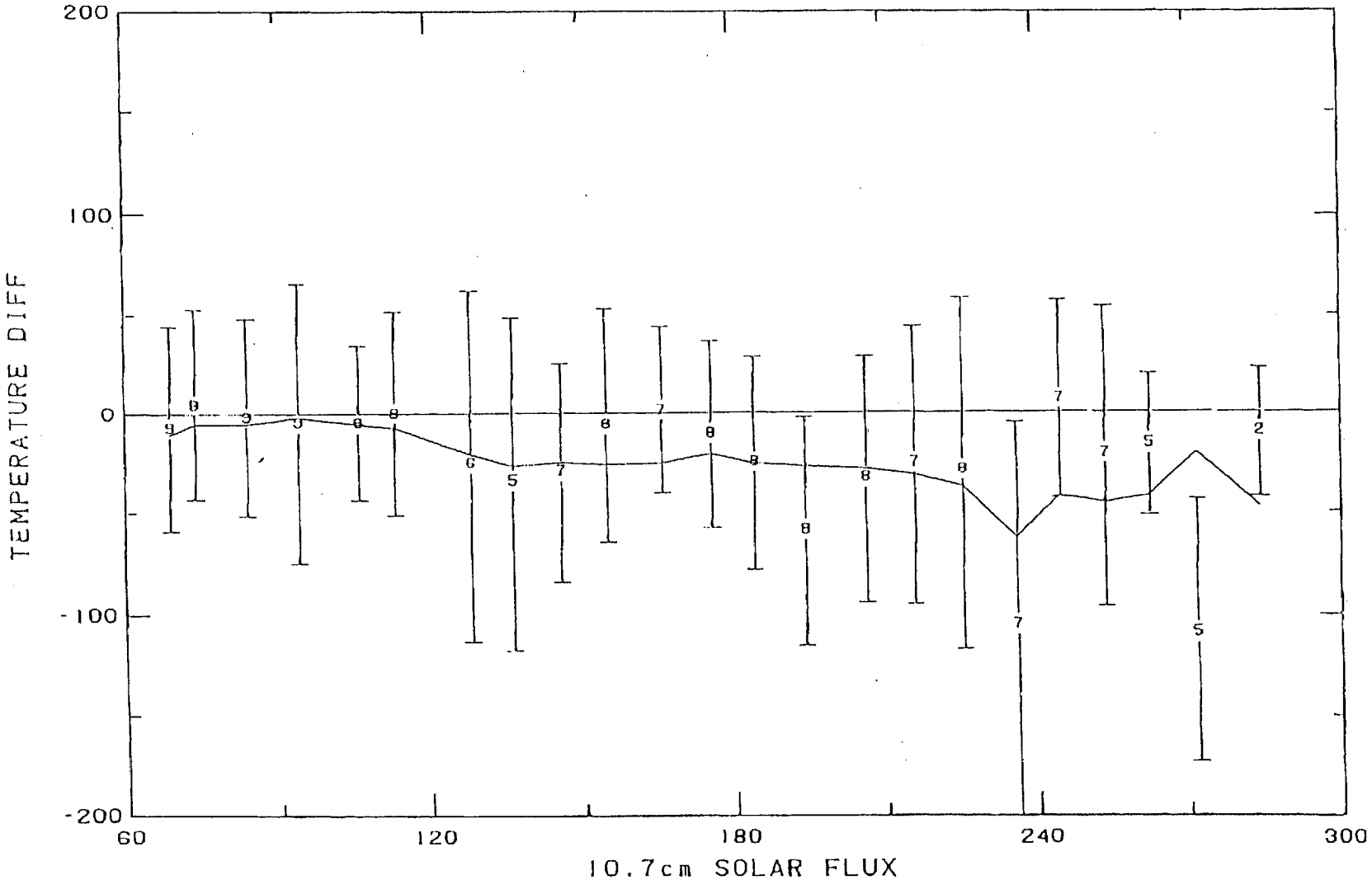

MS 0 GRP: 0 ALTL: -1.,1201.ISK: 43, 15. SEL: 0 0.0 0.0 PTS PLT: 6459 AVG: -11.90 SD: 60.29 A: 10.000 0.000
KP 0 SW: 1. 1. 1. 1. 1. 1. 1. 1.-1. 1. 1. 1. 1. 1. D1,D2: 81321 97182 ST,SX,SY 0 0 0 SN 1.00 DATA&MODEL 3 6
AVG,SD -23.6221 29.7966 AVXL,AVXH 0. 0. RMS 61.4531 DSD,MSD,R 166.6137 180.9986 0.99 KDM 4 ZANM 0
F 0.00(0.0) 0.00(0.0) 0.00(0.0) E15.883(51.1)14.564(33.3)14.827(10.8) M 0.00(0.0) 0.00(0.0) 0.00(0.0)AEX****

Fig 4(a)

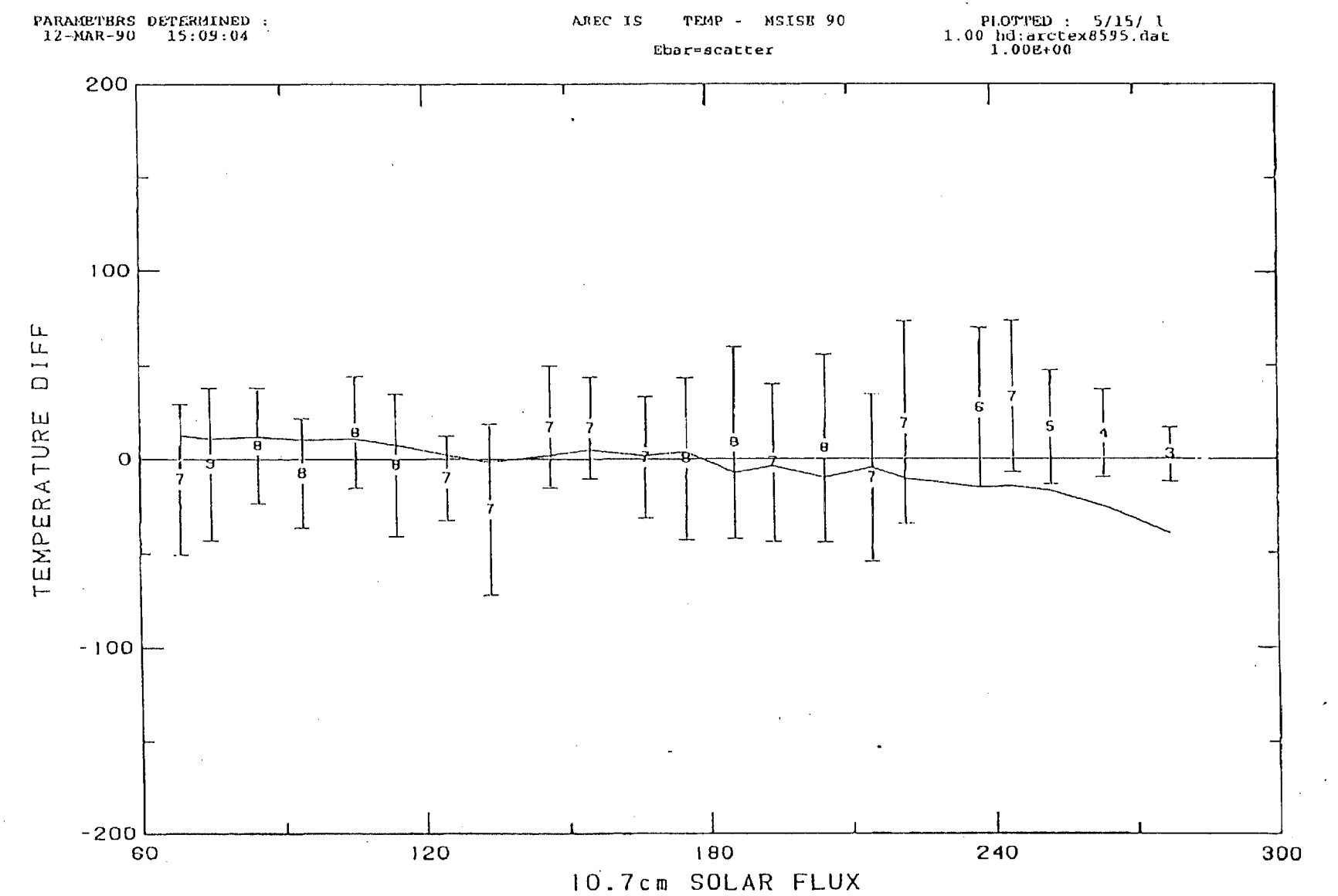

MS 0 GRP: 6 ALTL: -1.,1201.ISK: 0, 15. SBL: 0 0.0 0.0 PTS PLT: 3882 AVG: 4.40 SD: 41.44 A: 10.000 0.000
KP 0 SW: 1. 1. 1. 1. 1. 1. 1. 1.-1. 1. 1. 1. 1. 1. D1,D2: 85288 95126 ST,SX,SY 0 0 0 SM 1.00 DATA&MODEL 3 6
AVG,SD 5.1237 13.7555 AVXL,AVXH 0. 0. RMS 41.6759 DSD,MSD,R 152.3613 145.8864 1.00 KDN 4 ZANM 0
F 0.00(0.0) 0.00(0.0) 0.00(0.0) E 0.000(0.0) 0.000(0.0) 0.000(0.0) M 0.00(0.0) 0.00(0.0) 0.00(0.0)AEX****

Fig 4(b)

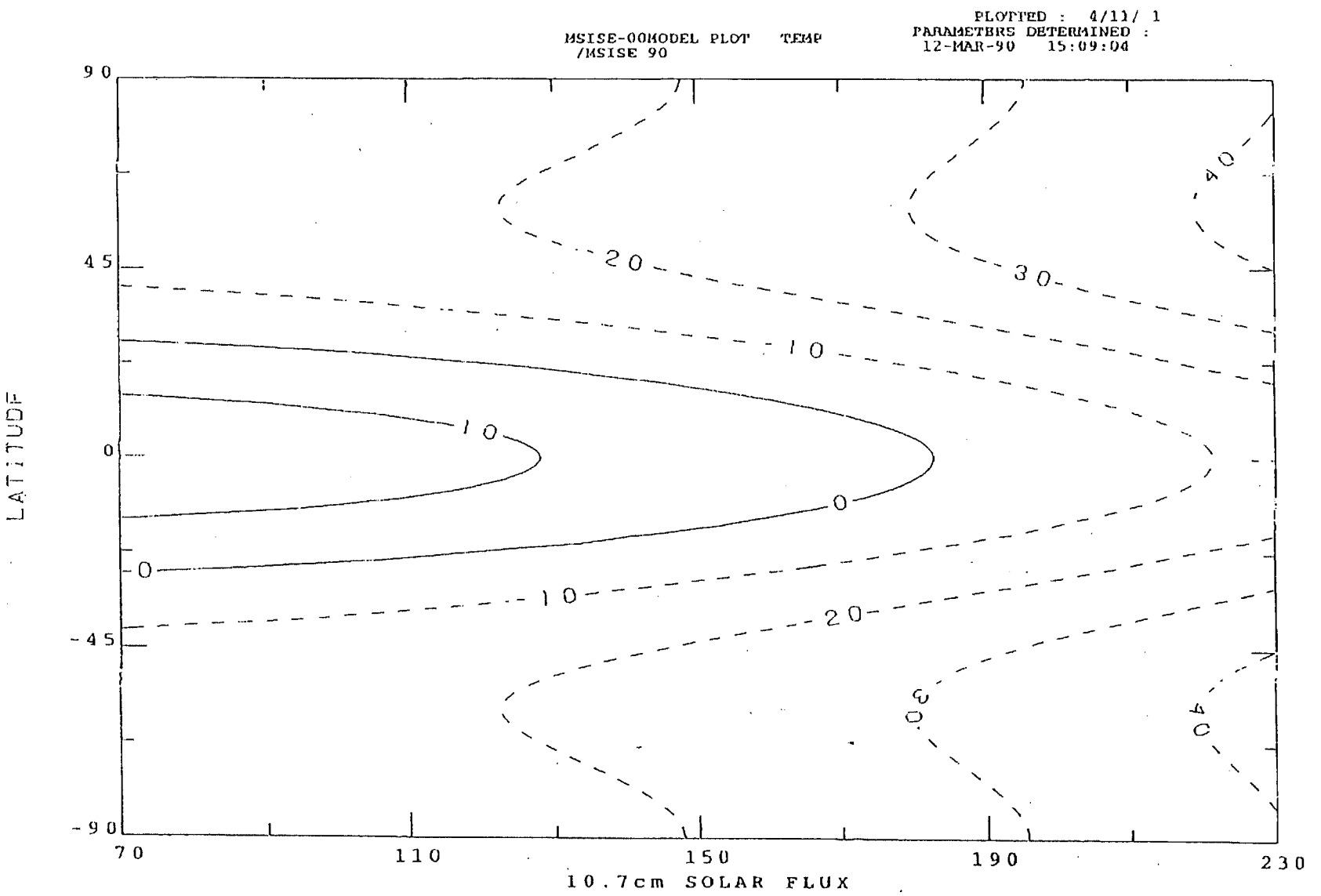
MSISE-00MODEL PLOT TEMP
/MSISE 90
PLOTTED : 4/11/ 1
PARAMETERS DETERMINED :
12-MAR-90 15:09:04
90
45
0
-45
-90
LATITUDE
70
110
150
190
230
10.7cm SOLAR FLUX
40
20
30
10
10
0
0
10
20
30
40
DAY= 0. LAT= 90. LT= 0.0 F107A=230. F107=233. AP= 4. ALT= 800. UT= 0. LONG= 0. A=-1.58E+01 P= 0.00E+00 SW:11000000 0.

Fig 5

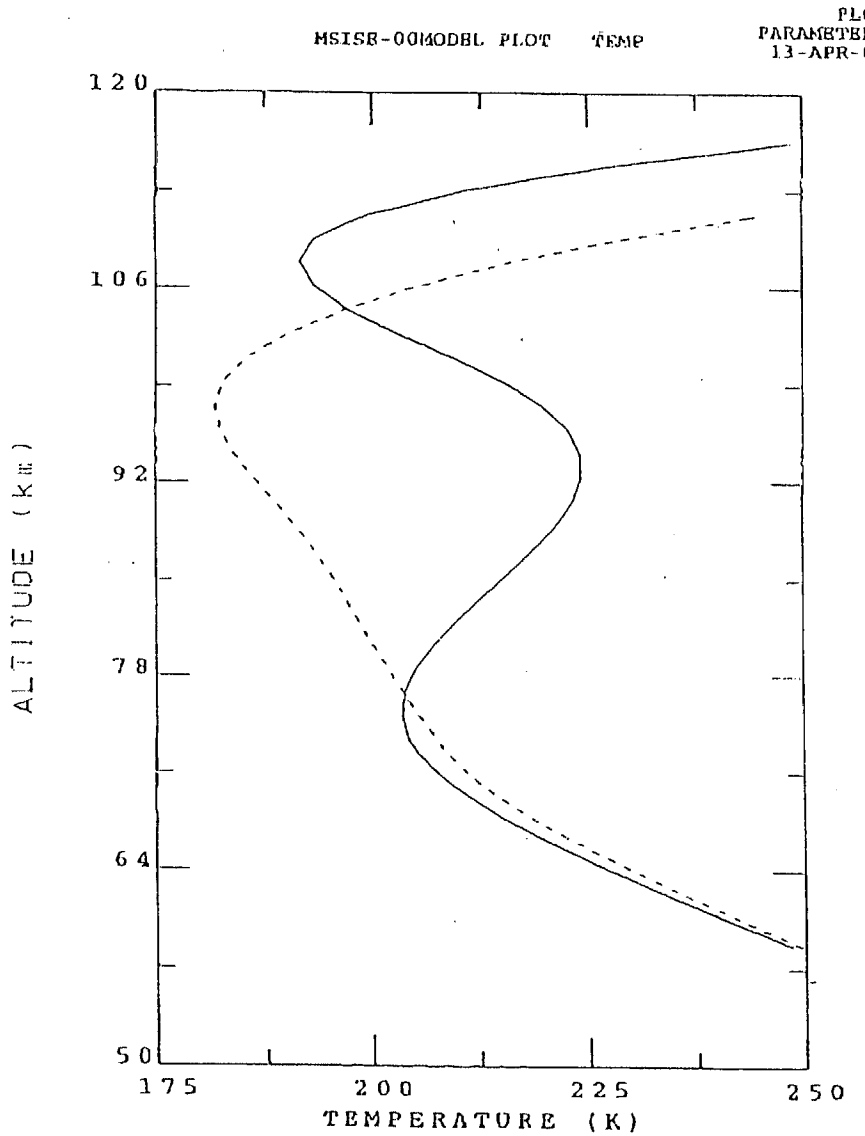

DAY= 90. LAT= 5. LT=21.0 F107A=150. F107=150. AP= 4. ALT= 122. UT= 0. LONG= 315. A= 8.33E+01 P= 0.00E+00 SW:11111111 111111

DAY= 90. LAT= 5. LT=21.0 F107A=150. F107=150. AP= 4. ALT= 122. UT= 0. LONG= 315. A= 8.10E+01 P= 0.00E+00 SW:11111111 111111

Fig 6(a)

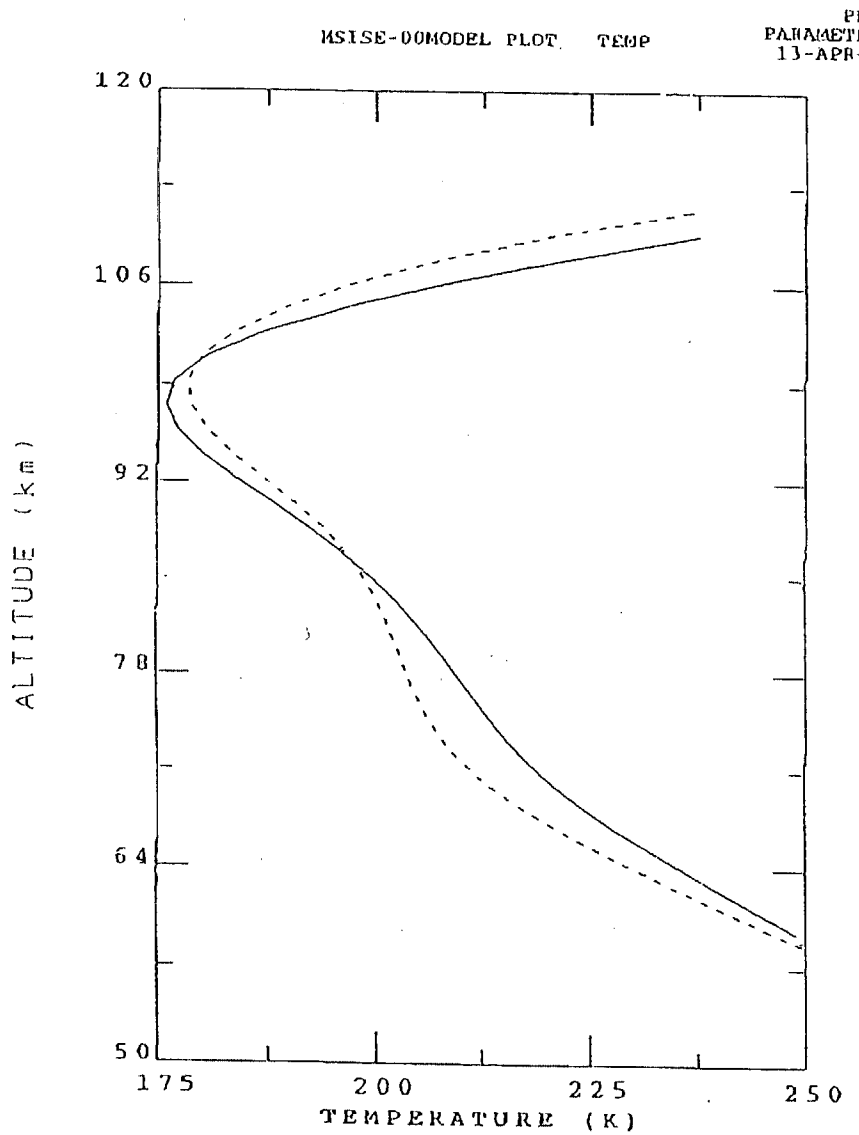

DAY= 90. LAT= 5. LT=10.0 F107A=150. F107=150. AP= 4. ALT= 122. UT= 0. LONG= 150. A= 8.07E+01 P= 0.00E+00 SW:11111111 111111

DAY= 90. LAT= 5. LT=10.0 F107A=150. F107=150. AP= 4. ALT= 122. UT= 0. LONG= 150. A= 8.10E+01 P= 0.00E+00 SW:11111111 111111

Fig 6(8)

Table 1(a). Comparison of models to drag, accelerometer, and rocket database on total mass density for quiet geomagnetic activity ($A_p \leq 10$)

Data Set*	ALT	PTS	M00		M90		J70	
			MEAN	SD	MEAN	SD	MEAN	SD
Jacchia drag	200 - 400	6236	-0.06	0.17	-0.06	0.17	-0.04	0.17
	400 - 800	10041	-0.07	0.23	-0.08	0.26	-0.07	0.25
	800 -1200	5586	0.01	0.23	0.03	0.27	-0.05	0.23
	>1200	15	0.20	0.09	0.27	0.10	-0.18	0.05
Barlier drag	120 - 200	2005	0.03	0.22	0.02	0.22	-0.07	0.22
	200 - 400	9343	0.04	0.21	0.04	0.20	0.03	0.22
	400 - 800	2880	0.12	0.32	0.10	0.32	0.17	0.33
Cactus accel	200 - 400	52722	-0.05	0.13	-0.06	0.13	-0.09	0.16
	400 - 800	52179	-0.05	0.19	-0.04	0.19	-0.07	0.22
SETA 79 accel	120 - 200	3792	0.03	0.07	0.06	0.07	-0.03	0.06
	200 - 400	4431	-0.04	0.17	-0.03	0.16	-0.04	0.17
SETA 82 accel	120 - 200	51329	-0.02	0.08	-0.03	0.09	-0.12	0.08
	200 - 400	54765	0.01	0.13	0.02	0.14	0.00	0.14
SETA 83 accel	120 - 200	44115	-0.08	0.08	-0.10	0.08	-0.17	0.08
	200 - 400	53888	-0.01	0.16	-0.04	0.16	-0.03	0.17
SETA 84 accel	120 - 200	40585	-0.12	0.08	-0.16	0.09	-0.24	0.08
	200 - 400	57258	-0.09	0.43	-0.12	0.43	-0.11	0.44
San Marco-5 accel	120 - 200	1882	0.37	0.15	0.29	0.16	0.37	0.15
	200 - 400	26070	0.18	0.20	0.14	0.19	0.19	0.30
	400 - 800	4192	0.10	0.34	0.12	0.33	0.46	0.52
AE-C MESA accel	120 - 200	23145	0.10	0.17	0.12	0.18	0.00	0.19
	200 - 400	12433	0.03	0.30	0.03	0.30	-0.01	0.30
AE-D MESA accel	120 - 200	15767	0.01	0.15	-0.03	0.16	-0.01	0.15
	200 - 400	4427	-0.05	0.20	-0.08	0.20	-0.04	0.20
AE-E MESA accel	120 - 200	25461	0.04	0.12	0.01	0.12	-0.03	0.14
	200 - 400	15190	0.07	0.24	0.02	0.23	0.03	0.25
rocket grenade	80 - 120	233	-0.04	0.16	-0.05	0.17	-0.12	0.19
rocket gauge	80 - 120	161	0.17	0.23	0.16	0.24	0.02	0.28
rocket drag (sphere)	80 - 120	135	0.03	0.19	0.05	0.17	-0.02	0.19
shuttle accel	80 - 120	61	-0.05	0.20	0.00	0.21	-0.11	0.16
	120 - 200	30	0.16	0.24	0.21	0.22	-0.08	0.23

* Complete drag and accelerometer data sets used for calculations

Table 1(b). Comparison of models to drag, accelerometer, and rocket database on total mass density for high geomagnetic activity ($A_p \geq 50$)

Data Set*	ALT	PTS	M00		M90		J70	
			MEAN	SD	MEAN	SD	MEAN	SD
Jacchia drag	200 - 400	304	-0.05	0.23	-0.07	0.23	-0.12	0.25
	400 - 800	441	-0.01	0.36	0.01	0.39	-0.17	0.42
	800 -1200	282	0.07	0.35	0.05	0.39	-0.14	0.39
Barlier drag	120 - 200	83	-0.09	0.19	-0.10	0.20	-0.12	0.20
	200 - 400	323	-0.11	0.22	-0.14	0.25	-0.13	0.23
	400 - 800	105	-0.12	0.47	-0.14	0.49	-0.18	0.48
Cactus accel	200 - 400	11497	0.04	0.20	0.04	0.19	-0.09	0.18
	400 - 800	4336	0.06	0.31	0.08	0.31	-0.15	0.29
SETA 79 accel	120 - 200	4310	0.00	0.11	0.01	0.11	0.01	0.09
	200 - 400	4382	-0.08	0.14	-0.07	0.14	-0.03	0.15
SETA 82 accel	120 - 200	21619	-0.04	0.12	-0.10	0.14	-0.06	0.13
	200 - 400	39907	-0.06	0.15	-0.10	0.18	-0.06	0.14
SETA 83 accel	120 - 200	14664	-0.08	0.09	-0.09	0.08	-0.10	0.09
	200 - 400	26103	-0.01	0.13	-0.04	0.14	0.00	0.13
SETA 84 accel	120 - 200	4848	-0.03	0.12	-0.10	0.10	-0.17	0.10
	200 - 400	14799	0.04	0.52	0.01	0.55	-0.03	0.52
San Marco-5 accel	200 - 400	366	0.29	0.14	0.28	0.14	0.45	0.15
	400 - 800	16	-0.24	0.41	-0.18	0.41	-0.03	0.41
AE-C MESA accel	120 - 200	4304	0.19	0.27	0.21	0.28	0.17	0.28
	200 - 400	1653	0.02	0.97	0.00	0.96	-0.05	0.97
AE-D MESA accel	120 - 200	199	0.25	0.13	0.15	0.12	0.19	0.14
	200 - 400	41	0.07	0.12	0.01	0.11	0.01	0.13
AE-E MESA accel	120 - 200	473	0.10	0.14	0.17	0.15	0.12	0.21
	200 - 400	133	0.13	0.38	0.14	0.39	0.10	0.36
rocket grenade	80 - 120	2	-0.22	0.01	-0.27	0.02	-0.27	0.02
rocket gauge	80 - 120	12	0.49	0.12	0.31	0.10	0.24	0.10
rocket drag (sphere)	80 - 120	2	0.25	0.01	0.27	0.00	0.20	0.01

* Complete drag and accelerometer data sets used for calculations

Table 1(c). Comparison of models to drag, accelerometer, and rocket database on total mass density across all geomagnetic activity levels

Data Set*	ALT	PTS	M00		M90		J70	
			MEAN	SD	MEAN	SD	MEAN	SD
Jacchia drag	200 - 400	10456	-0.07	0.17	-0.06	0.17	-0.07	0.19
	400 - 800	16021	-0.08	0.25	-0.07	0.27	-0.09	0.28
	800 -1200	9373	0.01	0.24	0.04	0.27	-0.07	0.25
	>1200	24	0.22	0.12	0.30	0.11	-0.20	0.13
Barlier drag	120 - 200	3285	0.01	0.22	0.00	0.23	-0.08	0.22
	200 - 400	14782	0.01	0.21	0.01	0.21	0.00	0.22
	400 - 800	4560	0.07	0.31	0.08	0.32	0.11	0.33
Cactus accel	200 - 400	52504	-0.05	0.14	-0.04	0.13	-0.09	0.17
	400 - 800	55760	-0.05	0.20	-0.01	0.20	-0.10	0.25
SETA 79 accel	120 - 200	30611	0.01	0.10	0.04	0.09	0.00	0.09
	200 - 400	32067	-0.07	0.15	-0.05	0.14	-0.04	0.16
SETA 82 accel	120 - 200	48445	-0.04	0.10	-0.06	0.11	-0.10	0.10
	200 - 400	51652	-0.03	0.14	-0.04	0.15	-0.04	0.14
SETA 83 accel	120 - 200	57350	-0.07	0.09	-0.10	0.09	-0.15	0.09
	200 - 400	54761	-0.01	0.16	-0.04	0.16	-0.02	0.17
SETA 84 accel	120 - 200	56816	-0.12	0.09	-0.16	0.09	-0.22	0.09
	200 - 400	44986	-0.09	0.40	-0.11	0.42	-0.11	0.42
San Marco-5 accel	120 - 200	2935	0.35	0.13	0.29	0.14	0.34	0.14
	200 - 400	41076	0.21	0.18	0.17	0.17	0.22	0.29
	400 - 800	7285	0.10	0.32	0.13	0.32	0.32	0.51
AE-C MESA accel	120 - 200	54353	0.11	0.17	0.14	0.17	0.06	0.19
	200 - 400	35842	0.03	0.30	0.03	0.30	-0.01	0.30
AE-D MESA accel	120 - 200	28499	0.01	0.16	-0.03	0.15	-0.01	0.15
	200 - 400	8170	-0.05	0.20	-0.07	0.20	-0.04	0.20
AE-E MESA accel	120 - 200	43798	0.05	0.12	0.03	0.13	-0.02	0.15
	200 - 400	24982	0.08	0.24	0.05	0.24	0.04	0.25
rocket grenade	80 - 120	310	-0.02	0.16	-0.03	0.16	-0.11	0.18
rocket gauge	80 - 120	247	0.21	0.24	0.20	0.25	0.07	0.27
rocket drag (sphere)	80 - 120	201	0.06	0.31	0.09	0.27	-0.01	0.28
shuttle accel	80 - 120	138	-0.07	0.19	0.00	0.20	-0.11	0.17
	120 - 200	52	0.07	0.23	0.13	0.21	-0.11	0.21

* Complete drag and accelerometer data sets used for calculations

Table 2(a). Comparison of models to temperature database for quiet levels of geomagnetic activity ($A_p \leq 10$)

Data Set	ALT	PTS	M00		M90		J70	
			MEAN	SD	MEAN	SD	MEAN	SD
Arecibo	120 - 200	20	5.12	78.23	-2.87	82.36	9.85	74.33
ISR	200 - 400	32	24.09	44.19	27.60	44.91	20.63	43.72
	400 - 799	42	72.16	94.17	79.40	94.31	75.17	91.21
	T_{ex}*	110	31.69	41.19	33.69	39.46	53.17	70.50
	T_{ex}**	186	-1.46	37.93	-3.86	38.90	-16.72	70.66
	T_{ex}***	1645	1.50	43.67	-1.84	41.27	-31.96	70.78
Millstone	100 - 130†	2498	-0.88	45.56	-3.34	43.58	4.57	50.76
Hill	T_{ex}†	287	41.01	50.81	25.41	48.65	55.51	78.11
ISR	T_{ex}††	232	-3.94	46.00	-30.15	47.06	-30.77	83.15
	T_{ex}†††	3082	3.70	47.74	-16.68	50.41	-9.50	84.09
St. Santin ISR	T_{ex}	303	6.15	44.78	-12.72	45.41	11.95	80.46
Jicamarca ISR	T_{ex}	33	-36.21	48.46	-35.25	48.81	-28.82	66.62
Malvern ISR	200 - 400	84	-16.24	67.98	-32.77	66.94	37.10	78.07
AE-C NATE	120 - 200	219	-39.52	111.18	-44.33	113.93	-10.61	111.94
NMS	200 - 400	212	-37.12	105.89	-41.93	107.78	-9.05	110.01
AE-D NATE	120 - 200	185	-28.58	103.34	-30.22	106.56	-12.58	107.63
NMS	200 - 400	217	-23.84	94.36	-26.24	94.36	7.69	107.97
AE-E NATE	120 - 200	329	-22.66	50.93	-29.09	52.23	-10.31	57.84
NMS	200 - 400	1003	-36.07	69.99	-32.18	70.39	-24.35	78.65
Rocket	120 - 200	140	-7.83	52.33	-5.79	55.20	11.39	59.69
NMS	200 - 400	82	-25.98	65.35	-32.61	69.22	0.52	59.28
DE-2 WATS	200 - 400	1723	-2.38	110.07	-21.19	109.37	-32.02	134.02
NMS	400 - 800	868	15.43	134.32	-4.14	133.26	-33.12	160.76

* Prior to 1985 (Data used to generate MSISE-90, NRLMSISE-00)
** 1985-95 (Data used to generate NRLMSISE-00)
*** 1985-95 (Entire new data set)
† Prior to 1981 (Data used to generate MSISE-90, NRLMSISE-00)
†† 1981-97 (Data used to generate NRLMSISE-00)
††† 1981-97 (Entire new data set)
‡ 1988-97 (LTCS 2-15: Concharenko and Salah [1998])

Table 2(b). Comparison of models to temperature database for high geomagnetic activity ($A_p \geq 50$)

Data Set	ALT	PTS	M00		M90		J70	
			MEAN	SD	MEAN	SD	MEAN	SD
Arecibo	120 - 200	12	-37.51	75.25	-45.49	72.28	-86.99	66.17
ISR	200 - 400	8	12.16	27.86	12.98	24.93	-22.05	41.96
	400 - 799	8	1.55	48.31	13.96	46.43	-70.11	55.65
	T_{ex}**	25	1.61	46.99	12.93	46.08	-43.05	56.16
	T_{ex}***	109	8.68	43.36	18.66	43.96	-60.08	56.61
Millstone	100 - 130††	97	-19.24	54.54	-19.18	49.92	-2.20	62.75
Hill	T_{ex}†	10	33.34	48.20	44.33	36.52	-6.35	57.86
ISR	T_{ex}††	130	3.83	121.84	-41.76	149.71	12.83	140.34
	T_{ex}†††	456	0.45	114.99	-46.39	138.81	10.31	125.38
St. Santin	T_{ex}	68	-21.43	79.14	-24.68	80.20	-66.08	88.88
ISR								
Malvern	200 - 400	7	-48.84	83.52	-51.66	84.04	-21.08	80.30
ISR								
AE-C NATE	120 - 200	62	-37.87	83.71	-40.82	83.71	-7.57	80.37
NMS	200 - 400	60	-232.70	259.42	-239.63	281.59	-248.31	266.39
AE-D NATE	120 - 200	14	23.31	46.07	49.94	42.61	48.59	65.00
NMS	200 - 400	25	-22.25	93.83	-19.14	100.11	118.77	113.96
AE-E NATE	120 - 200	25	-28.85	39.79	-32.13	40.37	-37.16	41.07
NMS	200 - 400	103	-90.40	152.53	-86.75	155.48	-144.90	157.64
DE-2 WATS	200 - 400	337	-457.87	602.70	-470.71	600.32	-395.19	531.19
NMS	400 - 800	190	-22.90	169.04	-37.49	173.60	43.21	189.20

* Prior to 1985 (Data used to generate MSISE-90, NRLMSISE-00)
** 1985-95 (Data used to generate NRLMSISE-00)
*** 1985-95 (Entire new data set)
† Prior to 1981 (Data used to generate MSISE-90, NRLMSISE-00)
†† 1981-97 (Data used to generate NRLMSISE-00)
††† 1981-97 (Entire new data set)
‡ 1988-97 (LTCS 2-15: Concharenko and Salah [1998])

Table 2(c). Comparison of models to temperature database across all levels of geomagnetic activity

Data Set	ALT	PTS	M00		M90		J70	
			MEAN	SD	MEAN	SD	MEAN	SD
Arecibo	120 - 200	55	3.28	80.48	-3.46	83.86	-9.39	87.31
ISR	200 - 400	98	26.28	42.01	28.99	41.97	18.82	51.86
	400 - 799	101	44.97	80.91	58.03	79.32	37.90	89.82
	T_{ex}*	172	31.12	46.26	36.19	45.19	34.79	79.02
	T_{ex}**	411	2.87	37.57	5.12	38.57	-26.29	57.73
	T_{ex}***	3882	2.87	42.04	4.40	41.44	-44.64	70.79
Millstone	100 - 130†	5352	-1.54	46.02	-2.70	44.57	11.53	52.27
Hill	T_{ex}†	559	41.35	58.15	30.50	54.37	51.30	87.22
ISR	T_{ex}††	583	-2.89	59.14	-24.72	67.77	-20.90	94.93
	T_{ex}†††	6459	4.76	55.74	-11.90	60.29	-4.27	88.18
St. Santin ISR	T_{ex}	642	-1.48	47.26	-16.83	46.67	-2.88	86.92
Jicamarca ISR	T_{ex}	52	-26.93	53.90	-24.84	54.29	-38.47	80.54
Malvern ISR	200 - 400	170	-20.82	71.20	-32.21	70.36	22.85	86.92
AE-C NATE	120 - 200	598	-39.19	101.03	-42.19	102.61	-7.73	101.78
NMS	200 - 400	571	-72.89	117.05	-73.10	118.07	-49.73	127.07
AE-D NATE	120 - 200	345	-26.49	96.02	-24.62	99.18	-5.34	101.72
NMS	200 - 400	437	-31.81	101.96	-28.17	101.61	10.90	124.55
AE-E NATE	120 - 200	664	-17.46	63.78	-22.81	63.88	-10.82	69.29
NMS	200 - 400	2158	-33.18	70.69	-27.12	71.60	-34.88	81.97
Rocket	120 - 200	185	-6.70	55.47	-6.02	60.40	4.44	63.49
NMS	200 - 400	111	-17.05	79.76	-23.69	84.06	2.30	78.43
DE-2 WATS	120 - 200	13	-76.32	548.69	-91.71	549.02	-24.64	523.71
NMS	200 - 400	4217	-20.49	143.93	-31.02	143.27	-36.83	165.84
	400 - 800	2213	5.37	142.22	-5.85	142.15	-19.93	169.57

* Prior to 1985 (Data used to generate MSISE-90, NRLMSISE-00)
** 1985-95 (Data used to generate NRLMSISE-00)
*** 1985-95 (Entire new data set)
† Prior to 1981 (Data used to generate MSISE-90, NRLMSISE-00)
†† 1981-97 (Data used to generate NRLMSISE-00)
††† 1981-97 (Entire new data set)
‡ 1988-97 (LTCS 2-15: Concharenko and Salah (1998))

Table 3(a). Comparison of models to database on N_2 concentration for quiet geomagnetic activity (Ap ≤ 10)

Data Set	ALT	PTS	M00		M90		J70	
			MEAN	SD	MEAN	SD	MEAN	SD
AEROS-A NMS	120 - 200	109*	0.09	0.16	0.11	0.16	0.10	0.16
	200 - 400	14018*	0.10	0.31	0.08	0.31	0.22	0.45
	400 - 800	4531*	0.24	0.53	0.17	0.53	0.90	0.79
OGO-6 NMS	200 - 400	69	0.11	0.17	0.01	0.16	-0.05	0.26
	400 - 800	1849	0.14	0.25	0.06	0.25	0.49	0.63
San Marco-3 NMS	120 - 200	9	0.05	0.12	-0.01	0.11	-0.04	0.14
	200 - 400	76	0.14	0.25	0.07	0.25	0.14	0.28
St. Santin ISR	80 - 120	272	-0.07	0.43	-0.05	0.45	-0.23	0.40
Arecibo ISR	80 - 120	211	-0.17	0.27	-0.17	0.27	-0.22	0.23
AE-C NATE NMS	120 - 200	10	-0.24	0.12	-0.14	0.10	-0.20	0.16
	200 - 400	1726	0.09	0.31	0.05	0.31	0.40	0.56
	400 - 800	234	0.26	0.40	0.18	0.39	1.08	0.69
AE-C OSS NMS	120 - 200	479	-0.06	0.15	-0.03	0.15	0.00	0.19
	200 - 400	949	-0.01	0.27	-0.04	0.27	0.16	0.38
AE-D OSS NMS	120 - 200	266	-0.03	0.16	-0.06	0.16	0.01	0.18
	200 - 400	238	-0.12	0.36	-0.17	0.37	0.02	0.50
AE-E NACE NMS	120 - 200	610	0.00	0.18	-0.01	0.16	-0.03	0.20
	200 - 400	1306	0.07	0.22	-0.01	0.22	-0.01	0.34
	400 - 800	838	0.09	0.26	-0.04	0.25	-0.14	0.36
Rocket UV occ	120 - 200	1	0.32	0.00	0.27	0.00	0.13	0.00
Rocket NMS	80 - 120	19	0.01	0.30	-0.02	0.30	-0.22	0.31
	120 - 200	225	-0.08	0.30	-0.08	0.30	-0.18	0.29
	200 - 400	87	-0.12	0.24	-0.11	0.25	-0.12	0.26
ESRO-4 NMS	200 - 400	1230	-0.12	0.31	-0.14	0.32	0.01	0.45
DE-2 NACS NMS	200 - 400	1955	-0.38	0.23	-0.41	0.23	-0.37	0.40
	400 - 800	520	-0.26	0.45	-0.33	0.43	-0.19	0.64
EISCAT ISR Averages	80 - 120	23	-0.08	0.17	-0.04	0.21	-0.16	0.11

*Entire data set

Table 3(b). Comparison of models to database on N_2 concentration for high geomagnetic activity ($A_p \geq 50$)

Data Set	ALT	PTS	M00		M90		J70	
			MEAN	SD	MEAN	SD	MEAN	SD
AEROS-A	200 - 400	3090*	-0.22	0.86	-0.21	0.86	0.02	0.92
NMS	400 - 800	1016*	-0.10	0.92	-0.09	0.94	0.52	1.30
OGO-6	200 - 400	9	0.09	0.23	0.04	0.22	-0.23	0.33
NMS	400 - 800	224	0.51	0.57	0.39	0.60	0.79	0.98
St. Santin ISR	80 - 120	34	0.00	0.36	0.00	0.35	-0.17	0.31
Arecibo ISR	80 - 120	31	-0.25	0.18	-0.26	0.21	-0.29	0.19
AE-C NATE	200 - 400	150	0.32	0.56	0.28	0.57	0.69	0.76
NMS	400 - 800	12	0.29	0.78	0.35	0.86	2.79	0.95
AE-C OSS	120 - 200	128	0.07	0.17	0.08	0.17	0.17	0.19
NMS	200 - 400	191	0.16	0.31	0.12	0.34	0.25	0.54
AE-D OSS	120 - 200	27	0.29	0.10	0.23	0.09	0.36	0.16
NMS	200 - 400	26	-0.05	0.23	-0.10	0.25	0.52	0.38
AE-E NACE	120 - 200	26	-0.01	0.16	0.08	0.15	-0.01	0.19
NMS	200 - 400	145	0.24	0.38	0.21	0.37	-0.13	0.39
	400 - 800	54	0.24	0.20	0.18	0.20	-0.28	0.35
ESRO-4 NMS	200 - 400	231	0.08	0.33	0.07	0.36	0.26	0.50
DE-2 NACS	200 - 400	570	-0.30	0.36	-0.36	0.36	-0.15	0.50
NMS	400 - 800	253	0.30	1.79	0.10	1.74	1.59	2.21

*Entire data set

Table 3(c). Comparison of models to database on N_2 concentration across all geomagnetic activity levels

Data Set	ALT	PTS	M00		M90		J70	
			MEAN	SD	MEAN	SD	MEAN	SD
AEROS-A	120 - 200	130*	0.09	0.15	0.11	0.15	0.12	0.16
NMS	200 - 400	38352*	0.04	0.34	0.04	0.34	0.21	0.49
	400 - 800	12342*	0.11	0.56	0.12	0.56	0.69	0.91
OGO-6	200 - 400	135	0.09	0.19	0.01	0.18	-0.11	0.34
NMS	400 - 800	3578	0.13	0.26	0.08	0.26	0.57	0.68
San Marco-3	120 - 200	16	-0.02	0.14	-0.07	0.14	-0.11	0.18
NMS	200 - 400	121	0.12	0.21	0.06	0.21	0.09	0.24
St. Santin ISR	80 - 120	558	-0.08	0.41	-0.05	0.42	-0.23	0.38
Arecibo ISR	80 - 120	403	-0.17	0.28	-0.17	0.29	-0.23	0.25
AE-C NATE	120 - 200	10	-0.23	0.12	-0.12	0.10	-0.20	0.16
NMS	200 - 400	3149	0.10	0.33	0.09	0.34	0.43	0.61
	400 - 800	472	0.24	0.45	0.24	0.46	1.20	0.81
AE-C OSS	120 - 200	1180	-0.05	0.16	-0.02	0.17	0.02	0.21
NMS	200 - 400	2271	0.01	0.28	0.00	0.28	0.17	0.42
AE-D OSS	120 - 200	507	0.00	0.16	-0.04	0.16	0.05	0.18
NMS	200 - 400	462	-0.13	0.35	-0.15	0.37	0.10	0.61
AE-E NACE	120 - 200	1076	-0.01	0.19	-0.01	0.17	-0.03	0.21
NMS	200 - 400	2712	0.07	0.25	0.01	0.25	-0.07	0.35
	400 - 800	1638	0.08	0.26	-0.02	0.26	-0.17	0.37
Rocket UV occ	120 - 200	2	0.02	0.26	0.02	0.23	-0.07	0.19
Rocket	80 - 120	32	-0.05	0.33	-0.08	0.35	-0.27	0.35
NMS	120 - 200	297	-0.06	0.30	-0.06	0.29	-0.16	0.29
	200 - 400	116	-0.20	0.55	-0.19	0.55	-0.21	0.50
ESRO-4 NMS	200 - 400	2621	-0.10	0.32	-0.11	0.34	0.08	0.47
DE-2 NACS	200 - 400	4971	-0.37	0.27	-0.39	0.26	-0.31	0.44
NMS	400 - 800	1544	-0.26	0.47	-0.32	0.47	-0.05	0.71
EISCAT ISR Averages	80 - 120	42	0.00	0.17	0.01	0.18	-0.16	0.14

*Entire data set

Table 4(a). Comparison of models to database on total oxygen concentration ($O+2O_2$) for quiet geomagnetic activity ($A_p \leq 10$)

Data Set	ALT	PTS	M00		M90		J70	
			MEAN	SD	MEAN	SD	MEAN	SD
AEROS-A	120 - 200	114*	0.24	0.10	0.21	0.10	-0.13	0.11
NMS	200 - 400	12021*	0.13	0.24	0.14	0.25	0.00	0.29
	400 - 800	8725*	0.12	0.37	0.11	0.37	0.16	0.38
OGO-6	200 - 400	67	0.06	0.12	0.06	0.11	0.12	0.15
NMS	400 - 600	1828	0.18	0.16	0.17	0.16	0.17	0.20
San Marco-3	120 - 200	21	-0.10	0.12	-0.13	0.11	-0.23	0.10
NMS	200 - 400	62	-0.04	0.16	-0.06	0.15	-0.09	0.17
AE-C NATE	200 - 400	1638	-0.09	0.18	-0.10	0.17	-0.15	0.22
NMS	400 - 600	272	-0.12	0.22	-0.15	0.20	-0.13	0.24
AE-C OSS	120 - 200	330	0.13	0.16	0.08	0.16	-0.15	0.24
NMS	200 - 400	873	0.05	0.24	0.04	0.24	-0.08	0.29
AE-D OSS	120 - 200	206	0.15	0.14	0.08	0.14	0.02	0.22
NMS	200 - 400	214	-0.03	0.25	-0.06	0.26	-0.11	0.31
AE-E NACE	120 - 200	292	-0.09	0.14	-0.12	0.13	-0.26	0.17
NMS	200 - 400	1411	-0.10	0.19	-0.11	0.19	-0.05	0.23
	400 - 600	893	-0.15	0.18	-0.17	0.17	-0.08	0.18
ESRO-4	200 - 400	1263	-0.17	0.24	-0.17	0.24	-0.26	0.27
NMS								
DE-2 NACS	200 - 400	2090	-0.12	0.17	-0.12	0.16	-0.09	0.26
NMS	400 - 600	1381	-0.06	0.24	-0.09	0.24	-0.08	0.26

*Entire data set

Table 4(b). Comparison of models to database on total oxygen concentration ($O+2O_2$) for high geomagnetic activity levels ($A_p \geq 50$)

Data Set	ALT	PTS	M00		M90		J70	
			MEAN	SD	MEAN	SD	MEAN	SD
AEROS-A	200 - 400	2096*	0.05	0.49	0.07	0.50	-0.10	0.60
NMS	400 - 800	1558*	-0.12	0.50	-0.08	0.51	-0.18	0.56
OGO-6	200 - 400	12	-0.01	0.14	0.01	0.16	0.04	0.25
NMS	400 - 600	137	0.18	0.18	0.19	0.19	0.18	0.22
AE-C NATE	200 - 400	203	-0.06	0.32	-0.05	0.32	-0.19	0.41
NMS	400 - 600	13	-0.26	0.16	-0.29	0.13	-0.25	0.17
AE-C OSS	120 - 200	142	0.23	0.18	0.15	0.19	-0.05	0.28
NMS	200 - 400	169	0.12	0.30	0.11	0.31	-0.18	0.48
AE-D OSS	120 - 200	20	0.22	0.17	0.02	0.18	-0.05	0.26
NMS	200 - 400	10	0.08	0.19	0.00	0.20	-0.16	0.38
AE-E NACE	120 - 200	7	-0.06	0.15	-0.01	0.15	0.05	0.27
NMS	200 - 400	133	-0.04	0.32	-0.04	0.32	0.08	0.43
	400 - 600	40	-0.10	0.20	-0.12	0.20	0.01	0.21
ESRO-4	200 - 400	234	-0.11	0.23	-0.11	0.23	-0.29	0.38
NMS								
DE-2 NACS	200 - 400	563	-0.16	0.23	-0.16	0.24	-0.29	0.39
NMS	400 - 600	389	-0.08	0.26	-0.08	0.27	-0.25	0.39

*Entire data set

Table 4(c). Comparison of models to database on total oxygen concentration ($O+2O_2$) across all geomagnetic activity levels

Data Set	ALT	PTS	M00		M90		J70	
			MEAN	SD	MEAN	SD	MEAN	SD
AEROS-A	120 - 200	135*	0.23	0.10	0.21	0.10	-0.12	0.11
NMS	200 - 400	30941*	0.08	0.25	0.10	0.25	-0.07	0.34
	400 - 800	22474*	0.01	0.38	0.04	0.38	0.03	0.43
OGO-6	200 - 400	156	0.01	0.14	0.01	0.14	0.05	0.21
NMS	400 - 600	3391	0.16	0.17	0.17	0.17	0.15	0.22
San Marco-3	120 - 200	31	-0.11	0.16	-0.14	0.14	-0.23	0.13
NMS	200 - 400	106	-0.05	0.14	-0.06	0.14	-0.09	0.16
AE-C NATE	200 - 400	3153	-0.09	0.19	-0.09	0.19	-0.16	0.25
NMS	400 - 500	521	-0.11	0.22	-0.12	0.21	-0.13	0.25
AE-C OSS	120 - 200	949	0.14	0.23	0.08	0.23	-0.14	0.29
NMS	200 - 400	2253	0.08	0.25	0.07	0.25	-0.08	0.33
AE-D OSS	120 - 200	392	0.15	0.15	0.05	0.15	-0.02	0.23
NMS	200 - 400	394	-0.03	0.24	-0.05	0.24	-0.14	0.32
AE-E NACE	120 - 200	545	-0.10	0.14	-0.13	0.13	-0.25	0.19
NMS	200 - 400	2851	-0.11	0.21	-0.11	0.21	-0.04	0.26
	400 - 600	1730	-0.16	0.19	-0.17	0.18	-0.07	0.20
ESRO-4	200 - 400	2592	-0.15	0.25	-0.15	0.25	-0.27	0.32
NMS								
DE-2 NACS	200 - 400	5141	-0.13	0.17	-0.13	0.17	-0.14	0.30
NMS	400 - 600	3525	-0.08	0.23	-0.09	0.23	-0.12	0.28

*Entire data set

Table 5(a). Comparison of models to database on helium concentration for quiet geomagnetic activity ($A_p \leq 10$)

Data Set	ALT	PTS	M00		M90		J70	
			MEAN	SD	MEAN	SD	MEAN	SD
AEROS-A	120 - 200	96*	0.71	0.32	0.74	0.32	-0.45	0.37
NMS	200 - 400	11814*	0.24	0.32	0.22	0.32	-0.06	0.90
	400 - 800	8543*	0.19	0.38	0.16	0.38	-0.13	0.79
OGO-6	200 - 400	35	0.20	0.15	0.18	0.15	0.25	0.38
NMS	400 - 800	1994	0.23	0.19	0.21	0.19	0.63	0.42
San Marco-3	120 - 200	13	0.45	0.27	0.44	0.28	0.06	0.19
NMS	200 - 400	91	0.15	0.21	0.14	0.22	-0.13	0.33
AE-C NATE	200 - 400	1706	-0.30	0.17	-0.32	0.18	-0.34	0.76
NMS	400 - 800	234	-0.29	0.18	-0.32	0.18	-0.02	0.73
AE-C OSS	120 - 200	339	-0.09	0.27	-0.08	0.28	-0.54	0.79
NMS	200 - 400	828	0.07	0.22	0.04	0.21	-0.29	0.92
AE-D OSS	120 - 200	192	-0.09	0.27	-0.12	0.27	-0.19	1.11
NMS	200 - 400	227	-0.23	0.38	-0.26	0.37	-0.24	1.25
AE-E NACE	120 - 200	257	0.12	0.22	0.10	0.22	-0.08	0.50
NMS	200 - 400	1416	-0.06	0.18	-0.07	0.18	-0.21	0.46
	400 - 800	845	-0.08	0.19	-0.10	0.20	-0.14	0.41
ESRO-4	200 - 400	1119	-0.13	0.32	-0.14	0.31	-0.34	1.06
NMS								
DE-2 NACS	200 - 400	1971	-0.13	0.16	-0.13	0.16	-0.12	0.71
NMS	400 - 800	1344	-0.12	0.16	-0.14	0.16	-0.25	0.56
	800 -1200	312	-0.06	0.20	-0.10	0.19	-0.28	0.39

*Entire data set

Table 5(b). Comparison of models to database on helium concentration for high geomagnetic activity ($A_p \geq 50$)

Data Set	ALT	PTS	M00		M90		J70	
			MEAN	SD	MEAN	SD	MEAN	SD
AEROS-A	200 - 400	2092*	0.31	0.95	0.28	0.95	-0.11	1.15
NMS	400 - 800	1566*	0.26	1.00	0.25	1.00	-0.18	1.11
OGO-6	200 - 400	13	0.03	0.09	0.02	0.12	0.45	0.41
NMS	400 - 800	140	1.40	1.49	1.41	1.50	1.82	1.39
AE-C NATE	200 - 400	174	-0.30	0.31	-0.32	0.31	-0.33	0.80
NMS	400 - 800	13	-0.30	0.23	-0.36	0.22	0.12	0.54
AE-C OSS	120 - 200	146	-0.06	0.45	-0.06	0.46	-0.60	0.89
NMS	200 - 400	202	-0.06	0.44	-0.08	0.46	-0.36	1.02
AE-D OSS	120 - 200	15	-0.08	0.31	-0.16	0.30	0.02	0.59
NMS	200 - 400	33	-0.20	0.31	-0.28	0.29	-0.17	0.65
AE-E NACE	120 - 200	8	0.17	0.11	0.16	0.12	0.79	0.26
NMS	200 - 400	131	-0.03	0.21	-0.06	0.20	0.20	0.49
	400 - 800	49	-0.13	0.12	-0.15	0.13	0.02	0.28
ESRO-4	200 - 400	211	-0.17	0.34	-0.18	0.34	-0.40	0.76
NMS								
DE-2 NACS	200 - 400	496	-0.16	0.26	-0.17	0.26	-0.40	0.64
NMS	400 - 800	572	-0.13	0.29	-0.12	0.33	-0.45	0.61
	800 -1200	44	-0.17	0.17	-0.19	0.18	-0.50	0.41

*Entire data set

Table 5(c). Comparison of models to database on helium concentration across all geomagnetic activity levels

Data Set	ALT	PTS	M00		M90		J70	
			MEAN	SD	MEAN	SD	MEAN	SD
AEROS-A	120 - 200	113*	0.72	0.31	0.76	0.31	-0.45	0.36
NMS	200 - 400	30166*	0.22	0.33	0.21	0.34	-0.16	0.89
	400 - 800	21840*	0.16	0.38	0.14	0.38	-0.15	0.77
OGO-6	200 - 400	68	0.17	0.15	0.14	0.14	0.40	0.43
NMS	400 - 800	3532	0.23	0.20	0.22	0.19	0.57	0.43
San Marco-3	120 - 200	26	0.45	0.23	0.43	0.23	0.04	0.19
NMS	200 - 400	145	0.13	0.19	0.11	0.20	-0.10	0.32
AE-C NATE	200 - 400	3277	-0.30	0.19	-0.31	0.19	-0.35	0.74
NMS	400 - 800	513	-0.29	0.19	-0.32	0.19	-0.06	0.71
AE-C OSS	120 - 200	964	-0.07	0.32	-0.07	0.33	-0.57	0.81
NMS	200 - 400	2219	0.05	0.27	0.03	0.26	-0.27	0.92
AE-D OSS	120 - 200	365	-0.08	0.30	-0.11	0.29	-0.17	1.10
NMS	200 - 400	435	-0.24	0.35	-0.27	0.33	-0.34	1.29
AE-E NACE	120 - 200	518	0.12	0.25	0.10	0.25	-0.03	0.52
NMS	200 - 400	2819	-0.05	0.17	-0.06	0.17	-0.14	0.47
	400 - 800	1661	-0.08	0.17	-0.09	0.17	-0.08	0.39
ESRO-4	200 - 400	2449	-0.14	0.31	-0.16	0.31	-0.42	1.03
NMS								
DE-2 NACS	200 - 400	4851	-0.12	0.18	-0.12	0.18	-0.18	0.67
NMS	400 - 800	4620	-0.13	0.19	-0.13	0.20	-0.32	0.56
	800 -1200	673	-0.09	0.18	-0.11	0.18	-0.35	0.40

*Entire data set

Table 6(a). Comparison of models to database on argon concentration for quiet geomagnetic activity ($A_p \leq 10$)

Data Set	ALT	PTS	M00		M90		J70	
			MEAN	SD	MEAN	SD	MEAN	SD
AEROS-A	120 - 200	109*	0.47	0.22	0.45	0.23	0.23	0.19
NMS	200 - 400	8565*	0.38	0.48	0.32	0.48	0.27	0.73
San Marco-3	120 - 200	11	0.58	0.21	0.50	0.20	-0.10	0.23
NMS	200 - 400	66	1.38	0.29	1.15	0.28	0.54	0.36
AE-C NATE	200 - 400	341	0.38	0.40	0.33	0.42	0.52	0.79
NMS								
AE-C OSS	120 - 200	299	-0.10	0.38	-0.07	0.38	-0.20	0.47
NMS	200 - 400	3	6.90	0.56	6.53	0.59	13.55	0.59
AE-D OSS	120 - 200	159	0.69	0.81	0.72	0.82	0.45	0.79
NMS								
AE-E NACE	120 - 200	313	-0.03	0.18	-0.01	0.18	-0.25	0.24
NMS	200 - 400	336	0.15	0.26	0.10	0.25	-0.13	0.31
Rocket	120 - 200	111	-0.13	0.66	-0.15	0.64	-0.42	0.67
NMS								
ESRO-4	200 - 400	1038	-0.15	0.40	-0.18	0.40	-0.12	0.78
NMS								
DE-2 NACS	200 - 400	1029	-0.01	0.43	-0.16	0.44	-0.11	0.78
NMS	400 - 800	18	5.00	1.08	3.70	1.10	9.19	0.99

*Entire data set

Table 6(b). Comparison of models tc database on argon concentration for high geomagnetic activity levels ($A_p \geq 50$)

Data Set	ALT	PTS	M00		M90		J70	
			MEAN	SD	MEAN	SD	MEAN	SD
AEROS-A NMS	200 - 400	1723*	0.58	1.53	0.57	1.52	1.12	1.81
AE-C NATE NMS	200 - 400	47	0.54	0.41	0.58	0.42	0.12	0.67
AE-C OSS	120 - 200	113	-0.01	0.50	0.14	0.50	0.43	0.64
NMS	200 - 400	4	74.95	2.16	69.97	2.01	88.57	1.91
AE-D OSS NMS	120 - 200	11	4.51	1.25	4.27	1.25	3.27	1.25
AE-E NACE	120 - 200	13	-0.18	0.13	-0.15	0.12	-0.46	0.21
NMS	200 - 400	58	0.55	0.79	0.58	0.76	-0.07	0.69
ESRO-4 NMS	200 - 400	223	-0.06	0.60	-0.07	0.59	0.55	1.07
DE-2 NACS	200 - 400	465	0.12	0.73	-0.09	0.76	1.27	1.12
NMS	400 - 800	81	1.18	1.00	0.45	1.10	12.77	1.22

*Entire data set

Table 6(c). Comparison of models to database on argon concentration across all geomagnetic activity levels

Data Set	ALT	PTS	M00		M90		J70	
			MEAN	SD	MEAN	SD	MEAN	SD
AEROS-A	120 - 200	130*	0.43	0.23	0.45	0.23	0.24	0.20
NMS	200 - 400	22539*	0.28	0.50	0.28	0.50	0.40	0.87
San Marco-3	120 - 200	22	0.53	0.19	0.51	0.18	-0.04	0.23
NMS	200 - 400	109	1.30	0.27	1.16	0.27	0.49	0.34
AE-C NATE	200 - 400	896	0.51	0.37	0.51	0.39	0.78	0.85
NMS								
AE-C OSS	120 - 200	802	-0.08	0.43	0.00	0.44	-0.02	0.59
NMS	200 - 400	25	2.63	2.10	2.57	2.14	3.37	2.46
AE-D OSS	120 - 200	287	0.56	0.77	0.61	0.78	0.40	0.79
NMS								
AE-E NACE	120 - 200	546	-0.08	0.25	-0.05	0.25	-0.28	0.29
NMS	200 - 400	719	0.16	0.39	0.14	0.39	-0.13	0.46
Rocket	80 - 120	23	-0.35	0.54	-0.38	0.53	-0.58	0.52
NMS	120 - 200	168	-0.14	0.52	-0.14	0.49	-0.36	0.55
	200 - 400	10	-0.34	0.02	-0.27	0.03	0.05	0.02
ESRO-4	200 - 400	2351	-0.19	0.44	-0.19	0.44	0.00	0.89
NMS								
DE-2 NACS	200 - 400	3045	-0.05	0.52	-0.15	0.53	0.23	0.96
NMS	400 - 800	170	1.22	1.01	0.64	1.10	8.32	1.17

*Entire data set

Table 7(a). Comparison of models to database on O_2 concentration for quiet geomagnetic activity ($A_p \leq 10$)

Data Set	ALT	PTS	M00		M90		J70	
			MEAN	SD	MEAN	SD	MEAN	SD
SMM[1]	120 - 200	42794[4]	-0.19	0.37	-0.40	0.37	-0.68	0.41
UV Occ	120 - 200	913	-0.08	0.25	-0.37	0.29	-0.66	0.35
	200 - 400	13043[3]	-0.23	0.62	-0.47	0.71	-0.69	0.78
AE-C OSS	120 - 200	60	-0.02	0.22	-0.10	0.24	-0.29	0.23
NMS	200 - 400	23	0.07	0.42	0.00	0.38	-0.12	0.43
AE-D OSS	120 - 200	219	0.24	0.34	0.19	0.34	0.01	0.36
NMS	200 - 400	71	0.11	0.36	0.13	0.36	0.05	0.42
AE-E OSS	120 - 200	112	0.24	0.22	0.18	0.22	-0.12	0.25
NMS	200 - 400	11	0.21	0.26	0.22	0.26	-0.06	0.28
Rocket Absorption	120 - 200	11	-0.12	0.30	-0.16	0.26	-0.41	0.32
Rocket	120 - 200	211	0.12	0.35	-0.02	0.32	-0.39	0.34
NMS	200 - 400	29	-0.13	0.57	-0.27	0.47	-0.55	0.44
AE-C EUVS	100	47	-0.09	0.22	-0.06	0.23	-0.20	0.26
UV Occ	130	20	0.26	0.19	0.27	0.20	-0.16	0.21
	150	61	0.19	0.28	0.08	0.28	-0.23	0.31
AE-E EUVS	100	114	0.03	0.33	-0.02	0.34	-0.06	0.32
UV Occ	130	77	0.01	0.19	-0.03	0.18	-0.43	0.21
	150[2]	72	-0.21	0.18	-0.33	0.17	-0.56	0.24
	150[3]	152	-0.06	0.20	-0.19	0.19	-0.47	0.25

[4] Entire data set; rows not marked relate to the subset of data selected to generate model.
[1] Solar Maximum Mission
[2] Channel 19
[3] Channel 06

Table 7(b). Comparison of models to database on O_2 concentration for high geomagnetic activity ($A_p \geq 50$)

Data Set	ALT	PTS	M00		M90		J70	
			MEAN	SD	MEAN	SD	MEAN	SD
SMM[1]	120 - 200	4136[4]	-0.25	0.55	-0.49	0.61	-0.69	0.65
UV Occ	120 - 200	183	-0.12	0.34	-0.44	0.46	-0.67	0.56
	200 - 400	1780[4]	-0.82	3.77	-0.88	3.83	-0.92	3.86
AE-C OSS	120 - 200	2	0.32	0.23	0.23	0.20	0.42	0.09
NMS	200 - 400	1	1.28	0.00	1.00	0.00	0.70	0.00
AE-C EUVS	100	8	0.08	0.22	0.06	0.20	-0.26	0.15
UV Occ	130	1	0.26	0.00	0.19	0.00	0.00	0.00
	150	7	0.32	0.39	0.11	0.39	0.27	0.38
AE-E EUVS	100	8	0.22	0.19	0.07	0.14	-0.05	0.12
UV Occ	130	8	0.09	0.15	0.04	0.16	-0.45	0.21
	150[2]	5	0.84	1.61	0.44	1.67	-0.19	1.63
	150[3]	15	-0.04	0.29	-0.21	0.30	-0.53	0.35

[4] Entire data set; rows not marked relate to the subset of data selected to generate model.
[1] Solar Maximum Mission
[2] Channel 19
[3] Channel 06

Table 7(c). Comparison of models to database on O_2 concentration across all geomagnetic activity levels

Data Set	ALT	PTS	M00		M90		J70	
			MEAN	SD	MEAN	SD	MEAN	SD
SMM[1]	120 - 200	51886[4]	-0.19	0.37	-0.42	0.40	-0.69	0.44
UV Occ	120 - 200	2091	-0.09	0.27	-0.38	0.32	-0.66	0.39
	200 - 400	27225[4]	-0.25	0.61	-0.52	0.72	-0.72	0.80
AE-C OSS	120 - 200	160	0.07	0.28	-0.02	0.28	-0.13	0.36
NMS	200 - 400	66	0.14	0.39	0.06	0.37	0.03	0.48
AE-D OSS	120 - 200	376	0.24	0.34	0.19	0.34	0.05	0.38
NMS	200 - 400	139	0.13	0.32	0.13	0.33	0.16	0.45
AE-E OSS	120 - 200	256	0.28	0.22	0.22	0.22	-0.11	0.25
NMS	200 - 400	47	0.15	0.29	0.15	0.29	-0.16	0.32
Rocket Absorption	120 - 200	14	-0.07	0.30	-0.12	0.27	-0.38	0.32
Rocket	80 - 120	37	-0.17	0.45	-0.22	0.45	-0.44	0.51
NMS	120 - 200	295	0.09	0.34	-0.04	0.31	-0.38	0.33
	200 - 400	44	-0.19	0.56	-0.31	0.45	-0.56	0.42
AE-C EUVS	100	121	0.00	0.23	0.04	0.24	-0.16	0.25
UV Occ	130	54	0.28	0.21	0.26	0.21	-0.09	0.24
	150	130	0.19	0.31	0.07	0.31	-0.15	0.38
AE-E EUVS	100	249	0.08	0.30	0.03	0.31	-0.05	0.29
UV Occ	130	175	0.00	0.20	-0.03	0.19	-0.43	0.22
	150[2]	163	-0.18	0.20	-0.32	0.19	-0.56	0.29
	150[3]	300	-0.05	0.21	-0.18	0.20	-0.48	0.27

[4] Entire data set; rows not marked relate to the subset of data selected to generate model.
[1] Solar Maximum Mission
[2] Channel 19
[3] Channel 06

Table 8(a). Comparison of models to database on atomic nitrogen concentration for quiet geomagnetic activity levels ($A_p \leq 10$)*

Data Set	ALT	PTS	M00		M90		J70	
			MEAN	SD	MEAN	SD	MEAN	SD
AE-C OSS	200 - 400	380	-0.11	0.44	0.11	0.44		
NMS	400 - 800	1994	-0.05	0.30	0.19	0.31		
AE-D OSS	200 - 400	2160	-0.42	0.29	-0.29	0.30		
NMS	400 - 800	871	-0.33	0.35	-0.16	0.36		
AE-E OSS	200 - 400	3998	0.04	0.27	0.12	0.27		
NMS								
DE-2 NACS	200 - 400	169	-0.75	0.72	-0.73	0.68		
NMS	400 - 800	74	-0.62	0.50	-0.59	0.47		

* Jacchia-70 model does not cover atomic nitrogen

Table 8(b). Comparison of models to database on atomic nitrogen concentration for high geomagnetic activity ($A_p \geq 50$)*

Data Set	ALT	PTS	M00		M90		J70	
			MEAN	SD	MEAN	SD	MEAN	SD
AE-C OSS	200 - 400	21	-0.15	0.38	-0.02	0.40		
NMS	400 - 800	335	0.00	0.38	0.18	0.40		
DE-2 NACS	200 - 400	54	-0.73	1.13	-0.69	1.08		
NMS	400 - 800	26	-0.07	1.27	-0.06	1.19		

* Jacchia-70 model does not cover atomic nitrogen

Table 8(c). Comparison of models to database on atomic nitrogen concentration across all geomagnetic activity levels*

Data Set	ALT	PTS	MOO		M90		J70	
			MEAN	SD	MEAN	SD	MEAN	SD
AE-C OSS	120 - 200	2	-0.96	0.26	-0.96	0.29		
NMS	200 - 400	670	-0.12	0.41	0.09	0.42		
	400 - 800	4538	-0.07	0.32	0.17	0.33		
AE-D OSS	200 - 400	3844	-0.42	0.31	-0.28	0.31		
NMS	400 - 800	1659	-0.37	0.39	-0.19	0.39		
AE-E OSS	200 - 400	7125	0.16	0.30	0.23	0.30		
NMS								
DE-2 NACS	120 - 200	103	-0.44	0.63	-0.38	0.63		
NMS	200 - 400	903	-0.61	0.81	-0.59	0.78		
	400 - 800	258	-0.46	0.73	-0.44	0.70		

* Jacchia-70 model does not cover atomic nitrogen

Table 9(a). Comparison of models to database on atomic hydrogen concentration for quiet geomagnetic activity levels ($A_p \leq 10$)*

Data Set	ALT	PTS	M00		M90		J70	
			MEAN	SD	MEAN	SD	MEAN	SD
AE-C BIMS	200 - 400	1756	0.03	0.30	0.05	0.31		
IMS	400 - 800	466	0.06	0.40	0.08	0.41		
AE-E BIMS	120 - 200	9	2.78	0.11	2.93	0.12		
IMS	200 - 400	1113	0.02	0.28	0.00	0.27		
	400 - 800	516	-0.08	0.31	-0.05	0.32		

* Jacchia-70 model does not cover atomic hydrogen

Table 9(b). Comparison of models to database on atomic hydrogen concentration for high geomagnetic activity levels ($A_p \geq 50$)*

Data Set	ALT	PTS	M00		M90		J70	
			MEAN	SD	MEAN	SD	MEAN	SD
AE-C BIMS	200 - 400	220	0.04	0.59	0.04	0.60		
IMS	400 - 800	65	-0.01	0.37	-0.02	0.36		
AE-E BIMS	200 - 400	71	0.16	0.48	0.13	0.47		
IMS	400 - 800	33	-0.19	0.29	-0.16	0.29		

* Jacchia-70 model does not cover atomic hydrogen

Table 9(c). Comparison of models to database on atomic hydrogen concentration across all geomagnetic activity levels*

Data Set	ALT	PTS	M00		M90		J70	
			MEAN	SD	MEAN	SD	MEAN	SD
AE-C BIMS	200 - 400	3735	0.06	0.32	0.07	0.33		
IMS	400 - 800	942	0.03	0.38	0.03	0.38		
AE-E BIMS	120 - 200	16	2.10	0.31	2.24	0.31		
IMS	200 - 400	2275	0.01	0.30	-0.01	0.30		
	400 - 800	1084	-0.11	0.34	-0.07	0.35		

* Jacchia-70 model does not cover atomic hydrogen

POPULAR SUMMARY

A new global, upper-atmospheric model is presented. This model is intended to replace previous models utilized in such applications as satellite orbit prediction. The new model termed the NRLMSISE-00 model, together with an associated database, NRLMSIS, is based on total mass densities from satellite accelerometers, satellite orbits, temperature determined by incoherent scatter, and molecular oxygen densities from the SMM solar occultation experiment. Extensive comparison is made with earlier upper atmospheric models such as MSIS and Jacchia-70. Model dependence on solar and geomagnetic activity is demonstrated more clearly than previous models. This model should become the standard for use in satellite orbit prediction.